NASA TECHNICAL NOTE

NASA TN D-2332

CONTROL-SURFACE INTERACTION EFFECTS ON DELTA-WING WINDWARD PRESSURES AT A MACH NUMBER OF 6.83 AT HIGH ANGLES OF ATTACK

by Luther Neal, Jr., and David E. Fetterman

Langley Research Center
Langley Station, Hampton, Va.

NATIONAL AERONAUTICS AND SPACE ADMINISTRATION • WASHINGTON, D. C. • JUNE 1964

CONTROL-SURFACE INTERACTION EFFECTS ON DELTA-WING WINDWARD PRESSURES AT A MACH NUMBER OF 6.83 AT HIGH ANGLES OF ATTACK

By Luther Neal, Jr., and David E. Fetterman

Langley Research Center
Langley Station, Hampton, Va.

NATIONAL AERONAUTICS AND SPACE ADMINISTRATION

For sale by the Office of Technical Services, Department of Commerce, Washington, D.C. 20230 -- Price $1.25

CONTROL-SURFACE INTERACTION EFFECTS ON DELTA-WING WINDWARD PRESSURES AT A MACH NUMBER OF 6.83 AT HIGH ANGLES OF ATTACK

By Luther Neal, Jr., and David E. Fetterman
Langley Research Center

SUMMARY

An experimental investigation has been conducted to determine the effects of nose incidence and trailing-edge-flap deflections on the windward pressure distribution over a 70° sweep delta wing at a Mach number of 6.83. The study was conducted over an angle-of-attack range from 30° to 90° with nose incidence of 0° to 20° and flap deflections of 10° to -90° at a Reynolds number of 0.6×10^6, based on mean aerodynamic chord.

Nose incidence produced large overexpansion effects on stations immediately behind the nose hinge line for the lower angles of attack, but did not significantly affect the pressure level over the rear portion of the wing. A similar overexpansion effect, produced by the middle panel, also occurred on negatively deflected flaps. These overexpansion effects were limited to angles of attack below about 70° and were not significantly affected by nose incidence. Large negative flap deflections caused a pressure reduction to occur ahead of the flap hinge line at the high angles of attack. Nose incidence had little effect on this flap-induced pressure reduction.

A region of separated flow, which was essentially two dimensional with nose incidence of 0°, existed ahead of the flap hinge line for a flap deflection of 10° up to angles of attack of about 60°. Because of the unfavorable pressure gradient resulting from overexpansion effects on the middle panel, nose incidence increased the extent of the separated-flow region as well as introducing considerably more three-dimensionality within the region of flow separation. Nose incidence also lowered the peak flap pressures which with nose incidence of 0° significantly exceeded the stagnation pressure behind a normal shock near an angle of attack of 50°.

INTRODUCTION

Because of the interest in delta wings for application to reentry vehicles capable of high-angle-of-attack reentry, a considerable amount of experimental data over a large angle-of-attack range has been published. (For example, see

refs. 1 to 4.) These investigations have been concentrated on determining the primary effects of angle of attack and leading-edge configuration on the heat transfer and pressure distributions on flat-plate wings. Little or no information, however, is available on the secondary effects induced by deflected control devices which are necessary to trim the vehicle. To obtain at least part of this information, an investigation of the windward pressures over a 70° delta wing was initiated at the Langley 11-inch hypersonic tunnel at a Mach number of 6.83 over an angle-of-attack range from 30° to 90°. Various nose incidences and trailing-edge-flap deflections were investigated. The integrated stability and control results of this investigation are reported in reference 5. The present report presents an analysis of the pressure distributions.

SYMBOLS

C_p	pressure coefficient, $\frac{p - p_\infty}{q_\infty}$
c	root chord
HL	hinge line
M_∞	free-stream Mach number
P	ratio of pressure on a surface behind an expansion to that on a surface without expansion at the same location and local angle of attack
p	surface pressure
p_∞	free-stream pressure
q_∞	free-stream dynamic pressure
x	distance along root chord measured from wing apex
y	spanwise distance measured from wing center line
α	angle of attack, angle between free-stream flow direction and plane of middle panel
α'	local surface angle of attack, $\alpha + \delta_f$
δ_e	expansion angle, $\delta_n - \delta_f$
δ_f	flap deflection, positive with trailing edge down
δ_n	nose incidence, positive with nose up
ϵ	angle between wing center line and rays passing through wing apex

ϵ' angle between wing center line and row of orifices parallel to leading edge, 20°

Λ leading-edge sweep angle

APPARATUS

Wind Tunnel

The tests were conducted in the Langley 11-inch hypersonic tunnel in a two-dimensional invar nozzle which provided a Mach number of 6.83 at the conditions of these tests. The core of uniform flow measures about $6\frac{1}{2}$ inches vertically and about 6 inches horizontally. Tunnel operation is of the intermittent type and test durations of about 80 seconds are possible. The variation in Mach number for the duration of a test run after the first 10 seconds of operation is about 1 percent. A calibration of the invar nozzle can be obtained from reference 6 and further details of the tunnel may be found in references 7 and 8.

Model and Model Support System

The basic dimensions of the model used in this investigation are given in figure 1, and a photograph of the model and model support strut are shown in figure 2. The model was constructed of steel and consisted of a delta wing with leading-edge sweep of 70° with a square leading-edge section. Both the nose section (16 percent of the total planform area) and the trailing-edge flap (36 percent of the total planform area) were deflectable. The clearance between the components at the hinges was about 0.005 inch. The upper and lower surfaces of the wing were ground parallel to facilitate setting of the nose incidence and flap deflection by means of steel angle braces (fig. 2) which were fastened to the upper surface of the wing.

The model support sting was attached to the tunnel angle-of-attack sector which rotated the model about a fixed point in the center of the test section over a pitch-angle range of 35°. This capability, in combination with the offset arm, which is shown in figure 2 and which allowed initial angle-of-attack settings of 30°, 60°, and 90°, permitted any angle of attack between 30° and 90° to be obtained.

INSTRUMENTATION

The model was equipped with 34 pressure orifices installed at the locations shown in figure 1 on the lower wing surface. These orifices were arranged in 10 longitudinal stations along three radial lines originating at the wing vertex (ϵ = 0°, 10°, 15°) and one row 0.04 inch from and parallel to the wing leading edge (ϵ' = 20°).

Because of the thinness of the model, it was impractical to conceal inside the model the pressure tubing which connected the pressure orifice to the measuring instrument. Instead, a typical pressure orifice in the region away from the leading edges was formed from 0.040-inch-inside-diameter tubing which projected through the upper wing surface and 18 inches into the support strut where it was connected to a 0.060-inch-inside-diameter tubing which formed the remainder of the pressure ducting system. A typical pressure orifice in the region near the leading edges was formed by drilling a 0.040-inch hole into a 0.040-inch-inside-diameter tubing installed in channels in the wing lower surface and covered with silver solder to form a smooth surface. These channels extended to the inner region of the wing where the 0.040-inch tubing was brought through the upper surface and routed as previously described. With this arrangement, the pressure tubes were shielded from the flow at all test angles of attack and thus were not expected to affect the pressures on the lower wing surface.

The pressure leads from the orifices were ducted through the model support system to the outside of the tunnel where the pressures were measured on aneroid-type six-cell recording units, described in reference 7. These units, which convert the deflection of a diaphragm into a rotation of a small mirror reflecting a beam of light onto a moving film, provide a time history of the measured pressure. The accuracy of these units is ±1/2 percent when the maximum capacity of the instruments is reached. At angles of attack near 90° the measured pressures approached the maximum range of most of the instruments. However, at an angle of attack of 30°, the accuracy was about ±2 percent on the main part of the wing and about ±5 percent over the streamwise flap. The stagnation pressure was read from a Bourdon tube gage at an accuracy of about ±1/2 percent.

TESTS

The tests were carried out at a stagnation pressure of 19 atmospheres, a corresponding Mach number of 6.83, and a stagnation temperature of 1,135° R. These test conditions resulted in a Reynolds number, based on mean aerodynamic chord, of 0.60×10^6. The high stagnation temperature was necessary to avoid air liquefaction in the test section. Water condensation effects were eliminated by keeping the absolute humidity of the air less than 1.87×10^{-5} pounds of water per pound of dry air for all tests.

The model angle of attack was varied from 30° to 90° at nose incidence settings of 0°, 10°, and 20° and trailing-edge flap deflections from 10° to -30°. Flap deflections of -50°, -70°, and -90° were also investigated at angles of attack above 65°. The flap deflection was set prior to each run and the angle-of-attack range was traversed at constant flap deflection. Three angles of attack were obtained during each run. Because of the short run duration, this procedure allowed about 20 seconds per angle of attack for the pressure instruments to reach equilibrium. Examination of the pressure records revealed that, in most cases, the pressure cells stabilized within 5 seconds after an angle-of-attack change; however, for streamwise or near-streamwise flap deflections, the pressure equilibrium time was somewhat longer and, in a very few cases, the pressures were still changing slightly at 20 seconds. To minimize the effects of

these few nonequilibrium cases, the values of the recorded pressures, used for data-reduction purposes, were selected at the end of the period of constant angle of attack. As a result of these separate periods of data reduction and the slight Mach number variation with time, quoted previously, the dynamic pressure uncertainty in the data is ±2 percent.

Schlieren photographs of the model were taken simultaneously with the pressure distributions. These photographs were used to measure the angles of attack by means of an optical comparator. By this method, the angles of attack were obtained to within $\pm 0.20^{\circ}$. Measurements of the model indicated that the angle braces allowed nose incidence and flap deflections to be set within $\pm 0.10^{\circ}$.

The gap at the hinges was unsealed for most of the tests; however, to determine the magnitude and nature of gap effects, representative runs were made with the gap sealed. The results of these tests indicated no measurable effects of the gap.

RESULTS AND DISCUSSION

Flow Visualization

Schlieren photographs.- Schlieren photographs of the model at various angles of attack are shown in figure 3 for representative nose incidences and flap deflections. For the basic wing ($\delta_n = \delta_f = 0^{\circ}$), the photographs in figure 3(a) and additional ones for intermediate angles of attack (not presented) show that the bow shock is straight, as is shown for $\alpha = 30^{\circ}$, up to an angle of attack of 55°. At $\alpha \approx 59^{\circ}$, however, slight curvature of the bow shock has occurred, and the curvature becomes more pronounced at higher angles of attack.

This bow-shock curvature may indicate that subsonic flow now exists over the wing. The fact that the local flow over the wing becomes subsonic at the angle of attack for the onset of shock curvature can be inferred from the behavior of the shock waves produced near the flap hinge line by the positively deflected flap ($\delta_n = 0^{\circ}$, $\delta_f = 10^{\circ}$; fig. 3(b)). At $\alpha \approx 40^{\circ}$, where local supersonic flow exists, an oblique shock is shown, and as the local surface Mach number decreases with increasing angle of attack a normal shock is approached at $\alpha = 55^{\circ}$. Between $\alpha = 55^{\circ}$ and 60°, the local flow becomes subsonic since no flap shock is evident at $\alpha = 60^{\circ}$. Reference 2 indicates that initial bow-shock curvature occurs at an angle of attack equal to the semicone angle for shock detachment which, for the Mach number of these tests, is about 56° and which agrees with the present results.

The flap shock at $\alpha \approx 40^{\circ}$ for $\delta_f = 10^{\circ}$ (fig. 3(b)) appears to originate at the hinge line. However, it is actually the shock from the boundary-layer reattachment point on the flap inasmuch as a region of separated flow existed ahead of the flap for angles of attack up to about 60° for all nose incidences. Unfortunately, this flow separation is not readily seen in figure 3(b), but its presence is confirmed by the results of oil-flow visualization tests which will be presented subsequently. At $\alpha \approx 50^{\circ}$ the shock near the hinge line starts

moving forward, and at $\alpha \approx 55^\circ$ the normal shock has moved considerably ahead of the hinge line. (See fig. 3(b).) This peculiar behavior at angles of attack near and above 50° is not thoroughly understood; however, it probably results from a combination of near-sonic local velocities and the presence of separated flow over the hinge line.

Nose incidence changes the shape of the bow shock ahead of the middle panel considerably at the lower angles of attack and also appears to reduce the strength of the normal hinge-line shocks at angles of attack near and above 50° for the positive flap deflection. However, above $\alpha = 60^\circ$, the effect of nose incidence on the shock patterns over the wing is small. Appreciable effects of negative flap deflections (fig. 3(c)) on the shock pattern ahead of the flap hinge line are limited to the high angle-of-attack regions where increases in shock curvature result.

Surface oil-flow studies.- Oil-flow patterns are shown in figures 4 and 5 for various nose incidences and flap deflections at representative angles of attack. These patterns were obtained by applying a mixture of oil and lamp black in discrete dots over the wing and exposing the model to the flow.

The model used for these tests differed somewhat from the pressure model previously described, in that the leading edge was about half as thick and was slightly rounded and the nose and flap components were not hinged. Instead, nose incidences and flap deflections were obtained by simply bending those portions of the model. The effect of the leading-edge differences on the resulting surface flows, at the angles of attack and most of the flap deflections considered here, is believed to be negligible for most cases. However, where the flap is near streamwise ($\alpha = 30^\circ$, $\delta_f = -30^\circ$; fig. 5(c)) the flow patterns over small regions near the flap tip may be somewhat affected. Through repeated bendings of the nose and flap components, slight surface concavities were formed at the nose and flap hinge lines and are clearly evident in figure 5. The depth of these concavities, however, was slight and, by comparing the photographs at $\alpha = 30^\circ$ and 60° in figure 5(a) with similar ones in figure 4 where no concavities exist, it is seen that their presence had a negligible effect on the surface flow patterns.

For the undeflected wing (fig. 4), the surface flow is essentially streamwise over most of the wing at $\alpha = 30^\circ$ but becomes radial at or before $\alpha = 40^\circ$. At $\alpha = 30^\circ$, a slight outflow can be noted in very small regions near the leading edge. This region of outflow increases in size with angle of attack until, at angles of attack of about 60° and higher, the entire wing is affected. At the extreme angles of attack (for example, $\alpha = 70^\circ$), the stagnation point has moved rearward from the apex. The rearward movement of the stagnation point continues with increasing angle of attack until, at $\alpha = 90^\circ$, the region of low shear appears to cover a large central portion of the wing.

This behavior of the surface flow patterns at the various angles of attack is almost the same as that on wings having larger and smaller leading-edge thicknesses (see refs. 1 and 3) and indicates the relative insignificance of leading-edge geometry on the surface flow characteristics at these angles of attack. An inviscid-flow theory for predicting the surface flow angles is included in

reference 1, but the theoretical values are significantly less than the experimental values over most of the angle-of-attack range. At $\alpha = 90^\circ$, however, the disk-transformation method proposed in reference 9 adequately predicts the surface flow. The results of this method are compared with the experimental results of the present investigation in reference 9.

The effects of nose incidence alone are shown in figure 5(a) for three angles of attack. At an angle of attack of 30°, increasing nose incidence promotes an inward flow tendency on the rearward portion of the model; this tendency becomes quite large for the model with nose deflection of 20°. This inward flow suggests the presence of a negative pressure gradient toward the center of the wing, the existence of which is borne out in the experimental pressure data to be presented in a subsequent section. At an angle of attack of 60°, the effects of increasing nose incidence are small, being limited mainly to small increases in the outward-flow angle near the leading edges. At an angle of attack of 90°, the deflected nose caused the nose hinge line to behave somewhat like an edge of the wing, thus providing a relieving effect which reduces the stagnation region over the central portion of the wing.

The most obvious effects of flap deflection is the separated-flow region formed ahead of the flap at $\delta_f = 10^\circ$ (fig. 5(b)) for angles of attack up to about 60°. For a nose incidence of 0°, the region appears to be essentially two dimensional except near the leading edges where relieving effects reduce the extent of separation. Nose incidence, however, apparently introduces considerably more three-dimensionality within the separated-flow region in addition to increasing the extent of the separated-flow region in the central portion of the wing.

In general, negative flap deflection (fig. 5(c)) does not appreciably affect the surface flow patterns over the forward portion of the model at angles of attack up to about 60°. At $\alpha = 90^\circ$, relieving effects near the flap hinge line for large negative flap deflection reduce the stagnation area in a manner similar to that observed near the nose hinge line for large nose incidence. Over the negatively deflected flap, the flow patterns are similar to those occurring over an undeflected wing at the same local angle of attack, except when nose incidence is employed, in which case inward-flow tendencies result at the lower angle of attack.

Pressure Distributions

A complete presentation of the large amount of local pressure data taken to obtain the integrated stability and control results presented in reference 5 would result in an unnecessary repetition of local pressure trends. Instead, these trends can be shown by considering only representative portions of the data at certain angles of attack and control deflections.

Basic delta wing.- The pressure distributions for the basic delta wing ($\delta_n = \delta_f = 0^\circ$) are shown in figure 6 for various angles of attack. Except near the nose and trailing edge of the wing, the center-line pressure coefficient is essentially constant for the lower angles of attack when the local flow field is

supersonic ($\alpha = 30^\circ$ to 55°). When the local flow field is subsonic, however, a negative pressure gradient exists along the wing, except at $\alpha \approx 90^\circ$, and severe pressure bleedoff occurs near the trailing edge. At $\alpha \approx 90^\circ$, because of the rearward movement of the stagnation point, extreme bleedoff in pressure occurs near both the apex and the trailing edge. The spanwise distributions indicate a relatively constant distribution at the lower angles of attack ($\alpha = 30^\circ$ to 40°) except for slight increases near the leading edge at $\alpha = 30^\circ$. At higher angles of attack, pressure reductions occur near the leading edges but, even up to $\alpha \approx 60^\circ$, the spanwise pressure is essentially constant over most of the wing.

The variation of the pressure coefficient with angle of attack for various x/c stations is shown more clearly in figure 7. The departure from essentially constant pressure along a given ray after the local flow becomes subsonic is quite apparent above $\alpha = 55^\circ$. Although a pressure gradient now exists over most of the wing, the most striking effect of the onset of subsonic flow is the sudden and severe pressure bleedoff near the trailing edge. This pressure bleedoff results in the forward center-of-pressure movement and unstable pitch tendencies shown for this wing in reference 5. The rearward movement of the stagnation point above $\alpha = 70^\circ$ is indicated by the angle of attack for peak pressures at the various stations along the wing.

Wing with nose incidence.- Representative pressure distributions for the wing with nose incidence is shown in figure 8 for $\delta_n = 20^\circ$. As would be expected, a discontinuity in the pressure coefficients occurs across the nose hinge line. As seen from the center-line pressure distributions at the lower angles of attack, the discontinuity is quite large, but generally tends to decrease as the angle of attack increases. Nose incidence also causes significant variations in the center-line pressure coefficient along the rest of the wing ($x/c > 0.4$) for angles of attack between about 35° and 55°.

The bleedoff in pressure near the leading and trailing edges of the wing (fig. 8) at the high angles of attack are similar to those shown for the undeflected wing in figure 6. For $\alpha \approx 30^\circ$, however, there appears to be more variation in spanwise pressure coefficients for rearward stations than for the undeflected wing. More discussion of the effects of nose incidence will be given in the section entitled "Interaction Effects."

Wing with flap deflection.- The pressure distributions for $\delta_f = 10^\circ$ and for a representative negative flap deflection ($\delta_f = -30^\circ$) are shown in figures 9 and 10. For the flap deflection of 10° (fig. 9), as should be expected when the local flow is supersonic, there is a rapid rise in chordwise pressure over the flap hinge line for angles of attack up to about 55°. The initial pressure rise occurs ahead of the hinge line as a result of the local flow separation shown previously in the surface oil-flow patterns.

It is also of interest to note that when the multiple shock system forms, as shown at $\alpha \approx 50^\circ$ in figure 3(b), the reattachment flap pressure exceeds the stagnation pressure behind a normal shock ($C_p \approx 1.82$). This high local pressure at reattachment may result in high local heating in this region. (See ref. 10.) Extreme pressure bleedoff at the trailing edge is seen to occur for angles of attack near 50°, with a resulting reduction of flap pitching-moment increments

for $\delta_f = 10^\circ$ in this angle-of-attack range as noted in reference 5. The spanwise pressure distributions (fig. 9) are similar to those for the undeflected wing except at the lower angles of attack for x/c greater than 0.75. The erratic behavior of the spanwise pressure distribution at these stations is due to the extent and distribution of the separated-flow region shown in figure 5(b).

The chordwise and spanwise pressure distributions over the negatively deflected flap (fig. 10) are essentially constant for angles of attack up to about 55°. Between $\alpha = 55^\circ$ and 70°, a positive pressure gradient exists over the flap immediately behind the hinge line, similar to that which occurred over the middle panel when the nose was deflected as shown in figure 8. For angles of attack above 70°, both the chordwise and spanwise pressure-bleedoff trends near the edges of the wing are similar to those for the undeflected wing as noted in figure 6.

Wing with both nose incidences and flap deflections.- The pressure distributions for typical combinations of nose incidence and flap deflection are presented in figure 11 (for $\delta_n = 20^\circ$, $\delta_f = 10^\circ$) and in figure 12 (for $\delta_n = 20^\circ$, $\delta_f = -30^\circ$). As would be expected, considerable pressure variation occurs along the wing; however, the behavior, in general, results from the superposition of the separate trends for a given nose incidence or flap deflection. Nevertheless, a few exceptions do occur, which will be pointed out in the next section.

Interaction Effects

The previous general discussion indicated several areas in which significant interactions between panels exist. As shown in reference 5, these interactions appreciably influence the force and moment characteristics of the wing.

Effects of nose incidence.- The effects of nose incidence on the pressure distribution for $\alpha \approx 35^\circ$ and 70°, which are representative of the medium and extreme angles of attack, are shown in figure 13 for typical flap deflections. At $\alpha \approx 70^\circ$, for all flap deflections, nose incidence produces no significant changes in the chordwise or spanwise pressure distributions behind the nose hinge line ($x/c > 0.4$). However, for $\alpha \approx 35^\circ$, as seen from the chordwise pressure distributions, nose incidence produces a large overexpansion[1] immediately behind the nose hinge line; the degree of overexpansion apparently increases with nose incidence. This overexpansion effect generally decreases with x/c, and with the flap undeflected (fig. 13(a)) the center-line pressures approach the basic-wing pressures near the trailing edge.

Nose incidence effects on the flap local pressures are also seen to occur at $\alpha \approx 35^\circ$ when the flap is deflected. With a negative flap deflection

[1]The term "overexpansion" as used herein refers to the condition wherein the local pressures on the surface behind an expansion are lower than those occurring at the same location on the undeflected wing at the same local angle of attack. Similarly the term "underexpansion" refers to the condition wherein higher local pressures result.

(fig. 13(b)) an underexpansion effect is seen in that the flap local pressures are increased slightly.[2] With a positive flap deflection (fig. 13(c)), however, because of the important influence of the separated-flow region (fig. 5(b)) and the multiple shock formations (fig. 3(b)), no particular pattern is evident.

The spanwise pressure distributions in figure 13 indicate that the overexpansion effect immediately behind the nose hinge line ($x/c = 0.45$) exists over the complete span. However, at stations further downstream, a spanwise positive pressure gradient exists, indicating that overexpansion effects are confined to the middle portion of the wing. The higher pressure near the leading edge apparently tends to raise the lower pressure near the center line at the more rearward stations and thus produces the inward surface flow patterns shown previously in figure 5 for $\alpha = 30^\circ$.

The angle-of-attack range in which overexpansion effects were encountered is shown in figure 14. Data are shown for the center line ($\epsilon = 0^\circ$) and the ray nearest the leading edge ($\epsilon' = 20^\circ$) at various chordwise stations. For the station behind the nose hinge line ($x/c = 0.45$), the overexpansion at both rays phases out when the local flow over the main portion of the wing becomes subsonic ($55^\circ < \alpha < 60^\circ$). At the more rearward stations ($x/c = 0.65$ and 0.85), however, as seen for $\delta_f = 0^\circ$ (fig. 14(a)), the overexpansion tends to phase out at lower angles of attack because of the chordwise pressure increases. The angle of attack at which the overexpansion effects disappear (for a given station) is apparently independent of the degree of nose incidence.

In addition to the overexpansion effect, nose incidence causes one additional effect worthy of note. The extreme flap pressure rise at $\alpha \approx 50^\circ$ which occurs at boundary-layer reattachment when $\delta_n = 0^\circ$ and $\delta_f = 10^\circ$ (fig. 9) does not occur when $\delta_n = 20^\circ$ (fig. 14(c)). This result further indicates that nose incidence tends to reduce the strength of the hinge-line normal shocks near $\alpha = 50^\circ$ as seen previously in the schlieren photographs in figure 3(b).

Effects of flap deflection.- Typical effects of flap deflection on the pressure distribution, with and without nose incidence, are shown in figure 15, again for the same two representative angles of attack. For $\delta_n = 0^\circ$ (fig. 15(a)), the negative flap deflection ($\delta_f = -30^\circ$) has no measurable effect on the chordwise or spanwise pressure ahead of the flap hinge line at the medium angle of attack ($\alpha \approx 35^\circ$). However, at $\alpha \approx 70^\circ$, there is a significant reduction in pressure ahead of the flap hinge line similar to that noted near the trailing edge of the undeflected wing in figure 6.

Deflecting the flap positively results in a pressure increase on the middle portion of the wing in the vicinity of the flap hinge line ($x/c = 0.75$) for both angles of attack. This increase in pressure at $\alpha = 70^\circ$ is not due to the presence of separated flow, as is the increase at $\alpha = 35^\circ$, but results from the higher pressure on the flap feeding forward in the local subsonic flow.

---

[2]This effect of nose incidence is seemingly contrary to that noted in the preceding paragraph. However, both effects are theoretically possible as will be shown in a subsequent discussion on carryover effects on the flap.

With a nose incidence of 20° (fig. 15(b)), flap-deflection effects similar to those noted in the preceding paragraphs are obtained. However, at $\alpha = 35°$, the positive flap deflection is seen to affect the pressure further forward on the wing because of the increase in extent of separated flow (see fig. 5(b)) due to nose incidence. This increase in separated flow with nose incidence is caused by the unfavorable pressure gradient which results from the nose induced overexpansion effect previously discussed.

It should be noted that an overexpansion effect is also produced on the negatively deflected flaps at certain angles of attack. This effect can be inferred by observing that the flap pressures immediately behind the flap hinge line at $\alpha = 70°$, $\delta_f = -30°$ are lower than those at $\alpha = 35°$, $\delta_f = 0°$ (fig. 15) despite the fact that the local flap angle of attack is 5° higher for $\alpha = 70°$, $\delta_f = -30°$.

The effects of flap deflection on the pressure coefficients for two chordwise locations and two rays ($\epsilon = 0°$ and $\epsilon' = 20°$) are shown in figure 16 as a function of angle of attack for nose incidences of 0° and 20°. At the forward location ($x/c = 0.55$) no significant effects due to flap deflections are noted up to angles of attack of about 55° for either nose incidence. Above $\alpha = 55°$, however, the pressure coefficients are slightly increased and decreased for the flap deflections of 10° and -30°, respectively. In front of the flap hinge line ($x/c = 0.75$), the flap deflection of 10° increases the pressure coefficients considerably throughout the entire angle-of-attack range whereas the flap deflection of -30° significantly reduces them above $\alpha = 55°$ but produces negligible effects below $\alpha = 55°$.

Carryover effects on the flap.- At certain angles of attack, as mentioned previously, overexpansion effects exist on the middle panel as a result of nose incidence. On the flap, however, conditions were shown wherein the local pressures were reduced (overexpansion[3]) whereas for other conditions the local pressures were increased (underexpansion). From this behavior, then, it is evident that the use of local-angle-of-attack theories, analogous to tangent-wedge or Newtonian concepts, may be invalid in most cases for predicting the pressures, or integrated forces, on surfaces in expanded flow. The extent and magnitude of deviations from a local-angle-of-attack analysis of the flap pressure at the station immediately behind the flap hinge line are shown for negative flap deflections in figure 17 for $\delta_n = 0°$ and 20° where C_p is plotted against the local angle of attack of the flap ($\alpha' = \alpha + \delta_f$). Data for an undeflected wing ($\Lambda = 75°$) from reference 9 at the same chordwise location are included to extend the data for $\delta_f = 0°$ to lower angles of attack. By using the data for $\delta_f = 0°$ as representative of the pressures existing on a surface without expansion, it is seen that flap overexpansion effects become significant at local angles of

[3]These overexpansion effects on the flap significantly reduced the stability at trim of the wing near the angle of attack for maximum lift coefficient (see ref. 5) whereas those on the middle panel had little effect on stability because of the shorter moment arm involved.

attack between about 20° and 60°, and the extent of overexpansion is relatively unaffected by nose incidence. Below $\alpha = 20°$ and above 60°, however, the data indicate that some underexpansion (higher pressure) is occurring and the effect is increased by nose incidence at local angles of attack below 20°.

In order to gain some insight into these overexpansion or underexpansion effects, inviscid-flow calculations of the local pressures in the expanded regions of the model were made. These calculations were carried out for various degrees of expansion δ_e, various local angles of attack α', and various Mach numbers. Both two-dimensional shock theory and conical shock theory were used to determine the local conditions over the surface ahead of the expanded regions; then the flow was expanded two dimensionally. The resulting pressure was normalized by the corresponding pressure (predicted by either two-dimensional or conical shock theory) which occurs on a surface without expansion at the same local angle of attack. The pressure ratio so obtained is denoted P and is shown in figure 18 as a function of free-stream Mach number for various expansion angles and local angles of attack.

For the two-dimensional shock analysis, at a local angle of attack of 0°, only an underexpansion effect ($P > 1$) is seen which increases rapidly with both expansion angle δ_e and Mach number. As the local angle of attack increases, however, the degree of underexpansion becomes smaller and P becomes less sensitive to changes in δ_e and Mach number. In addition, a slight amount of overexpansion ($P < 1$) is seen for $\delta_e = 10°$.

For the conical shock analysis (fig. 18(b)) similar effects of δ_e and Mach number on P are seen throughout the local angle-of-attack range. The degree of underexpansion, however, is reduced at the lower local angles of attack and significant regions of overexpansion are seen to occur throughout the local angle-of-attack and expansion-angle ranges. Because of the radial nature of the flow patterns seen in figure 4 and because the leading-edge shock is attached at the model vertex but detached at the leading edges, it is believed that the conical shock analysis is more representative of the experimental results presented herein. The previously discussed regions of overexpansion or underexpansion, produced by nose incidence and/or flap deflection are therefore explainable and depend on the amount of expansion and the local angle of attack. Experimental values of P which were obtained by normalizing with the data for $\delta_n = \delta_f = 0°$ in figure 17 are also included in figure 18(b). In general, reasonably good agreement occurs with the conical shock results except at the lower local angles of attack where boundary-layer effects become important.

CONCLUDING REMARKS

An experimental investigation has been conducted to determine the effects of nose incidence and trailing-edge flap deflections on the windward pressure distribution of a 70° sweep delta wing at a Mach number of 6.83 and for an angle-of-attack range from 30° to 90°. From the results of the investigation the following remarks apply:

At angles of attack up to about 55°, the pressure distributions were essentially constant over most of the wing when no controls were deflected. Immediately after the onset of local subsonic flow over the wing (at angles of attack between 55° and 60°), a significant pressure bleedoff occurred near the wing trailing edge. At higher angles of attack, considerable pressure variation, both chordwise and spanwise, prevailed over the entire wing.

Nose incidence produced large overexpansion effects on the middle panel below an angle of attack of 60°; similar effects were introduced by the middle panel on negatively deflected flaps in the same general angle-of-attack range. At higher angles of attack, large negative flap deflections caused a pressure reduction ahead of the flap hinge line. This behavior was similar to the severe pressure bleedoff that occurred at the trailing edge of the undeflected delta wing. Nose incidence, however, had little effect on either the pressure bleedoff or the flap overexpansion effects.

For a positive flap deflection of 10°, the flow separated ahead of the flap hinge line for angles of attack up to about 60°. Below an angle of attack of 40°, the separation region was essentially two dimensional for a nose incidence of 0°. Nose incidence introduced considerably more three-dimensionality within the separated-flow region as well as increasing the extent of the separation because of the unfavorable pressure gradient resulting from nose overexpansion effects on the middle panel. Nose incidence also lowered the peak flap pressures which with a nose incidence of 0° significantly exceeded the stagnation pressure behind a normal shock near an angle of attack of 50°.

Langley Research Center,
National Aeronautics and Space Administration,
Langley Station, Hampton, Va., February 12, 1964.

REFERENCES

1. Dunavant, James C.: Investigation of Heat Transfer and Pressures on Highly Swept Flat and Dihedraled Delta Wings at Mach Numbers of 6.8 and 9.6 and Angles of Attack to 90°. NASA TM X-688, 1962.

2. Clark, E. L., and Spurlin, C. J.: The Aerodynamic Characteristics of a 75-Deg Swept Delta Wing at High Angles of Attack and Mach Numbers of 2 to 8. AEDC-TDR-62-99 (Contract No. AF 40(600)-800 S/A 24(61-73)), Arnold Eng. Dev. Center, May 1962.

3. Bertram, Mitchel H., and Everhart, Philip E.: An Experimental Study of the Pressure and Heat-Transfer Distribution on a 70° Sweep Slab Delta Wing in Hypersonic Flow. NASA TR R-153, 1963.

4. Mueller, James N. (With appendix by Eugene S. Love): Pressure Distributions on Blunt Delta Wings at a Mach Number of 2.91 and Angles of Attack up to 90°. NASA TM X-623, 1962.

5. Fetterman, David E., and Neal, Luther, Jr.: An Analysis of the Delta-Wing Hypersonic Stability and Control Behavior at Angles of Attack Between 30° and 90°. NASA TN D-1602, 1963.

6. Bertram, Mitchel H.: Exploratory Investigation of Boundary-Layer Transition on a Hollow Cylinder at a Mach Number of 6.9. NACA Rep. 1313, 1957. (Supersedes NACA TN 3546.)

7. McLellan, Charles H., Williams, Thomas W., and Bertram, Mitchel H.: Investigation of a Two-Step Nozzle in the Langley 11-Inch Hypersonic Tunnel. NACA TN 2171, 1950.

8. McLellan, Charles H., Williams, Thomas W., and Beckwith, Ivan E.: Investigation of the Flow Through a Single-Stage Two-Dimensional Nozzle in the Langley 11-Inch Hypersonic Tunnel. NACA TN 2223, 1950.

9. Bertram, Mitchel H., and Henderson, Arthur, Jr.: Recent Hypersonic Studies of Wings and Bodies. ARS Jour., vol. 31, no. 8, Aug. 1961, pp. 1129-1139.

10. Becker, John V., and Korycinski, Peter F.: Heat Transfer and Pressure Distribution at a Mach Number of 6.8 on Bodies With Conical Flares and Extensive Flow Separation. NASA TN D-1260, 1962.

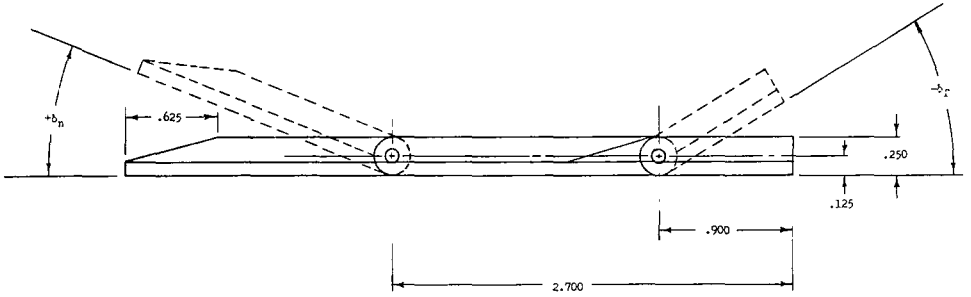

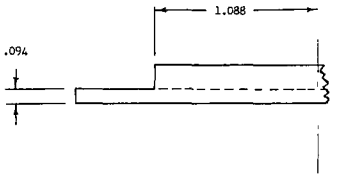

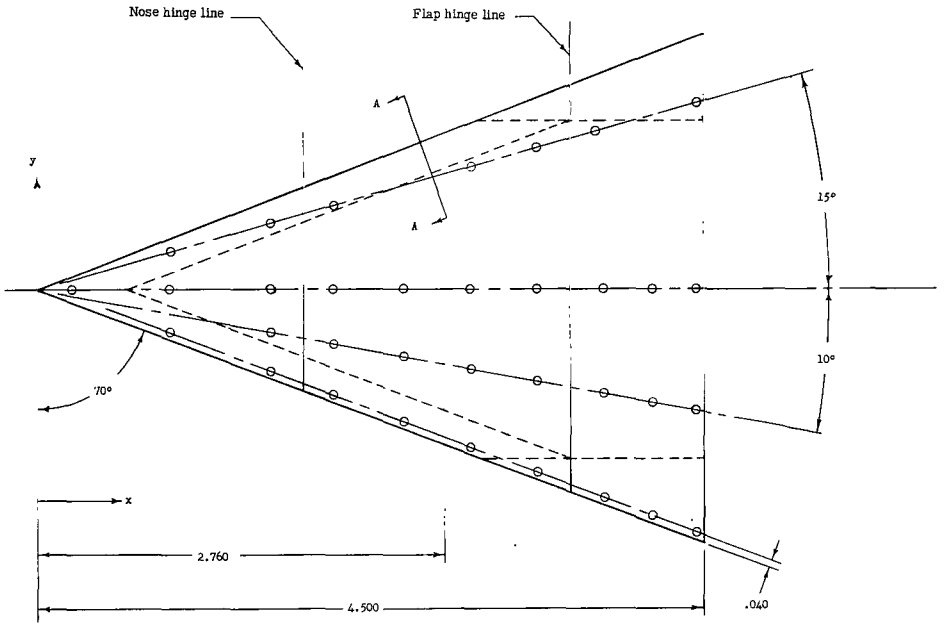

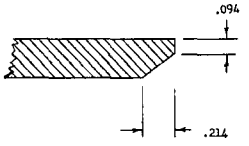

Section A-A

Orifice locations

Station	x/c		y/c		
1	.050		0		
2	.200	.054	0		-.065
3	.350	.094	0	-.064	-.118
4	.450	.121	0	-.076	-.154
5	.550		0	-.097	-.191
6	.650	.174	0	-.115	-.227
7	.750	.201	0	-.132	-.263
8	.850	.227	0	-.150	-.300
9	.920		0	-.162	-.325
10	.990	.265	0	-.175	-.351

Figure 1.- Model dimensions and orifice locations. All dimensions are in inches.

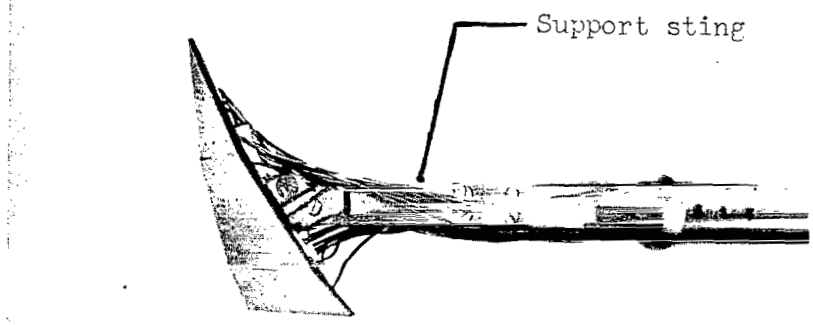

(a) Three-quarter front view.

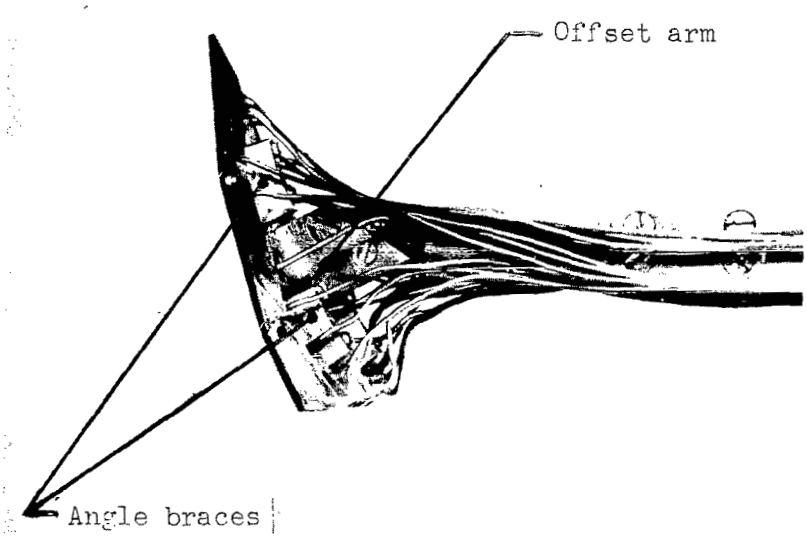

(b) Three-quarter rear view.

Figure 2.- Photograph of model and model support strut. L-62-7043

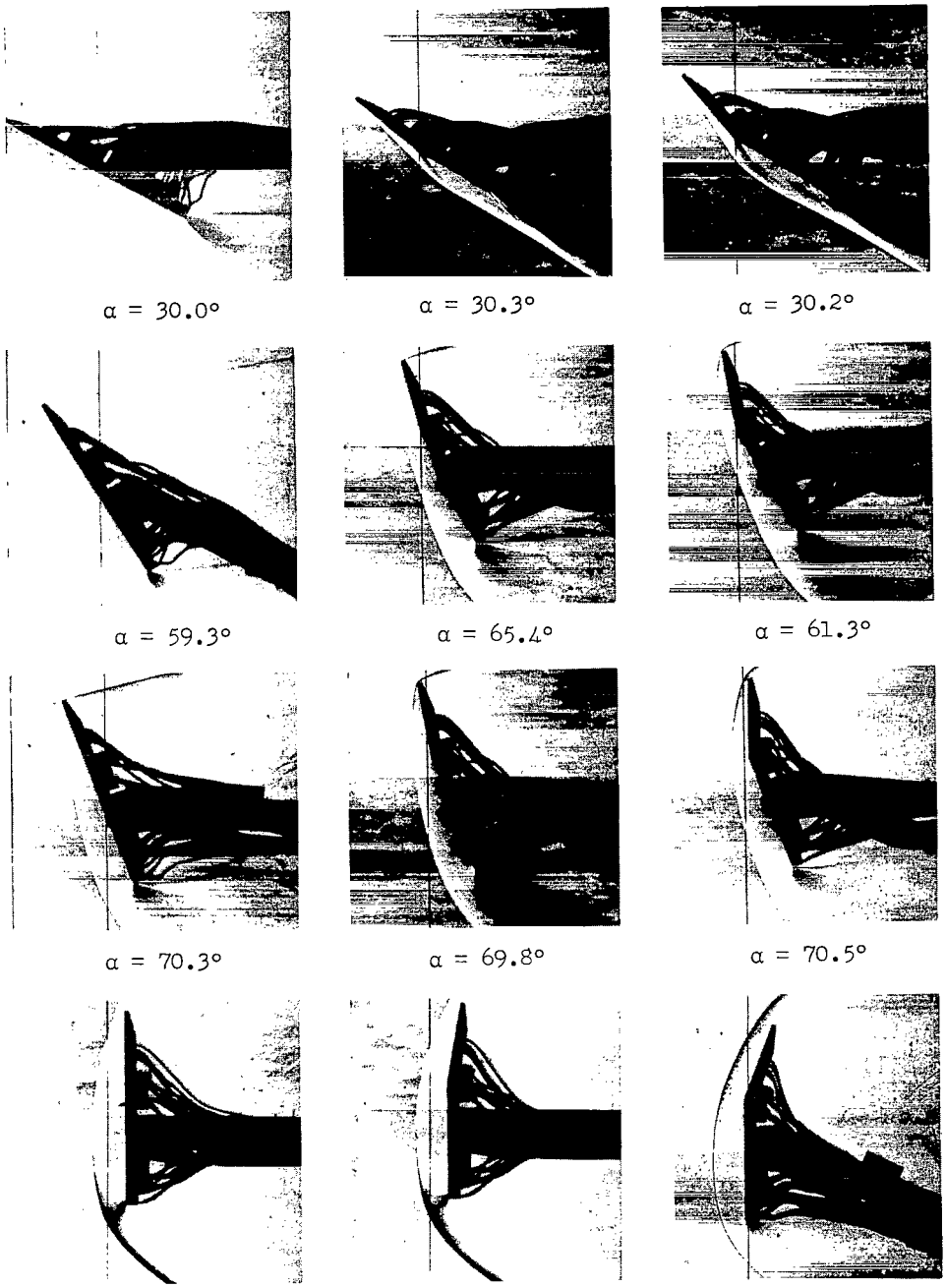

(a) $\delta_f = 0^o$.

Figure 3.- Schlieren photographs of model. L-62-7045

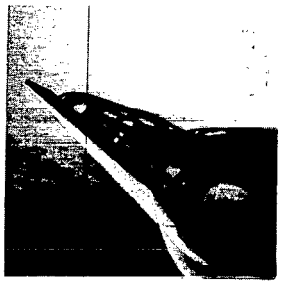

$\alpha = 40.4°$

$\alpha = 40.1°$

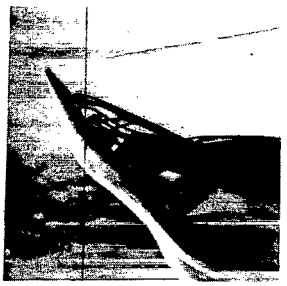

$\alpha = 40.2°$

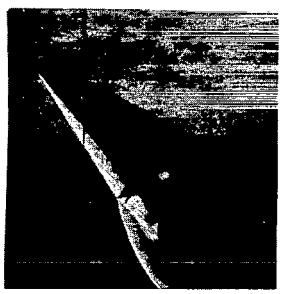

$\alpha = 49.9°$

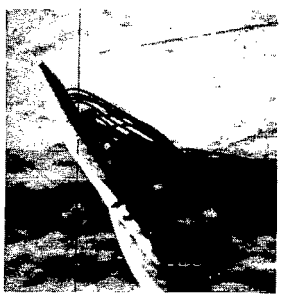

$\alpha = 50.2°$

$\alpha = 49.7°$

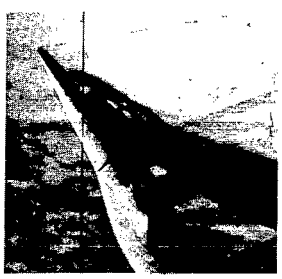

$\alpha = 55.0°$

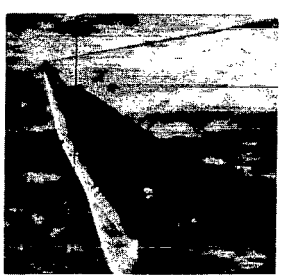

$\alpha = 55.1°$

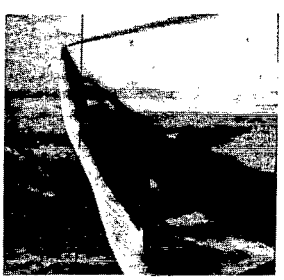

$\alpha = 55.3°$

$\alpha = 60.0°$

$\delta_n = 0°$

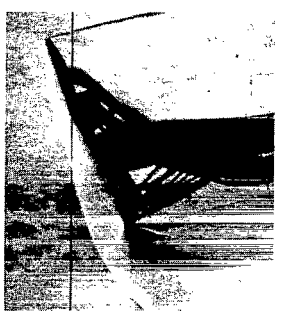

$\alpha = 60.6°$

$\delta_n = 10°$

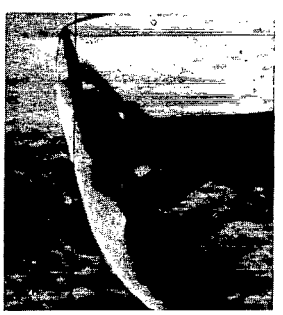

$\alpha = 60.3°$

$\delta_n = 20°$

(b) $\delta_f = 10°$.

Figure 3.- Continued.

L-62-7044

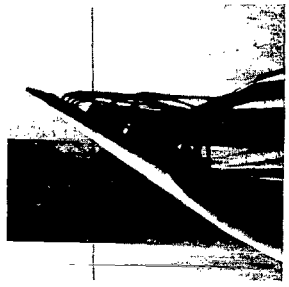

$\alpha = 30.5°$

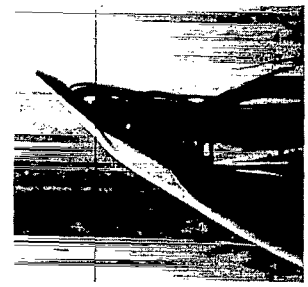

$\alpha = 30.4°$

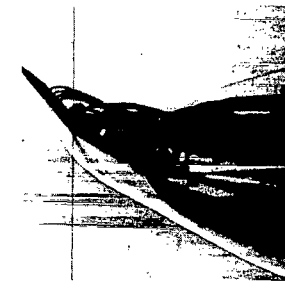

$\alpha = 30.8°$

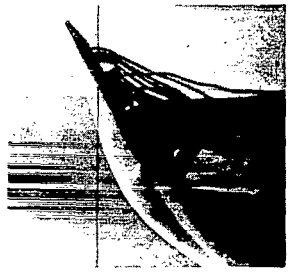

$\alpha = 62.5°$

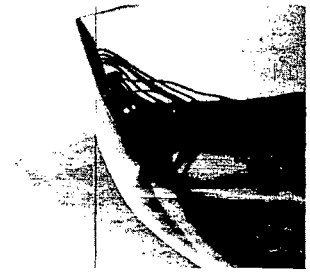

$\alpha = 62.3°$

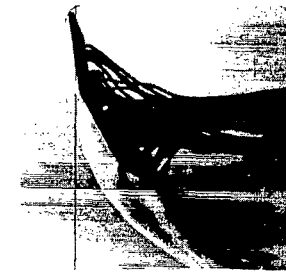

$\alpha = 62.5°$

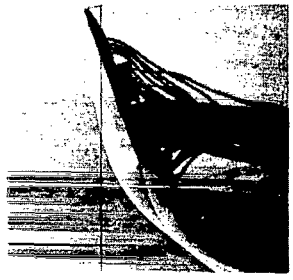

$\alpha = 71.2°$

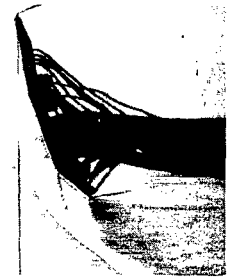

$\alpha = 71.0°$

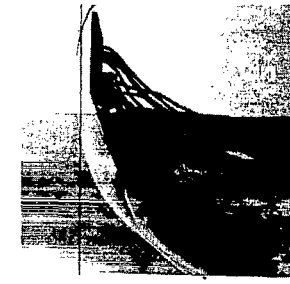

$\alpha = 70.8°$

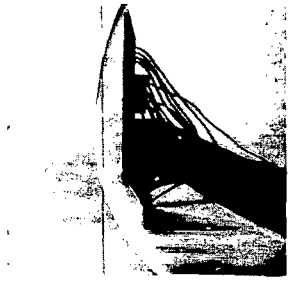

$\alpha = 90.9°$

$\delta_n = 0°$

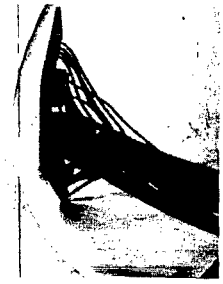

$\alpha = 90.6°$

$\delta_n = 10°$

$\alpha = 90.3°$

$\delta_n = 20°$

L-62-7046

(c) $\delta_f = -30°$.

Figure 3.- Concluded.

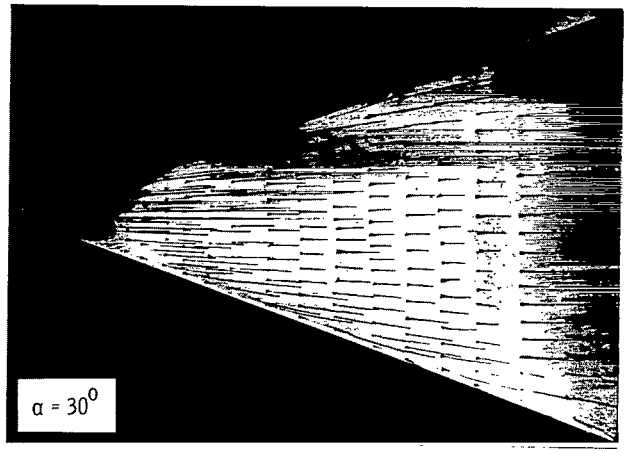

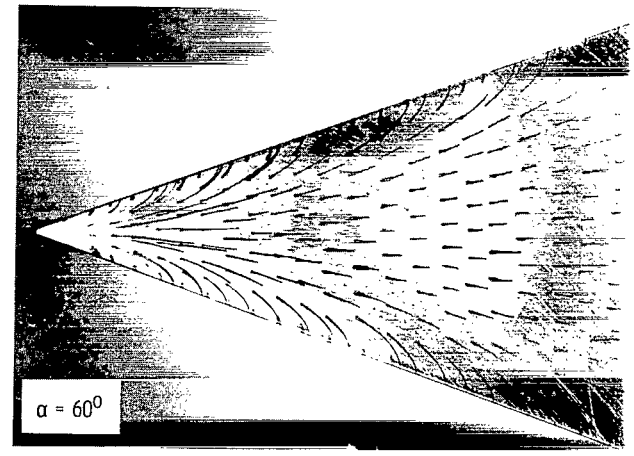

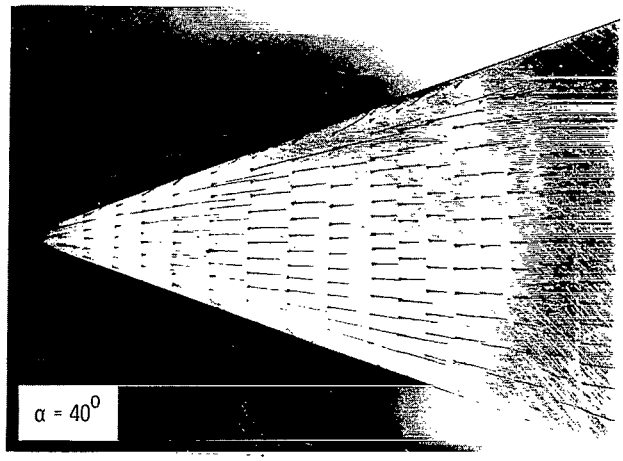

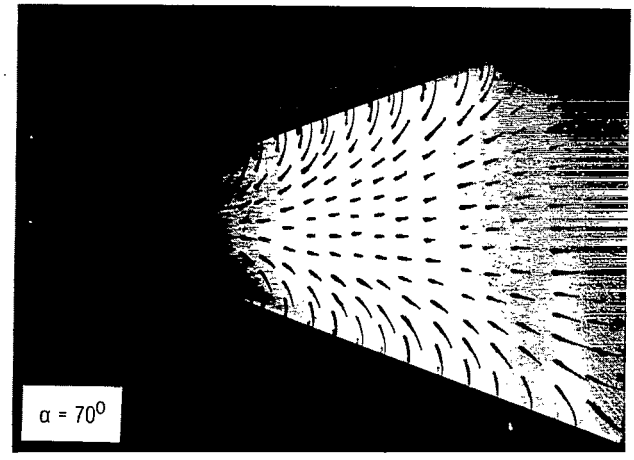

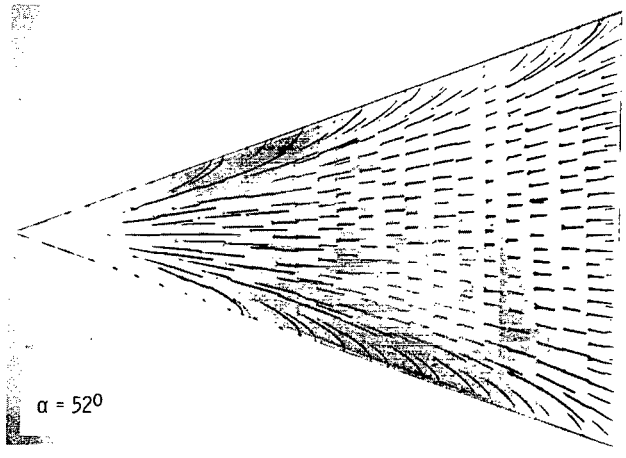

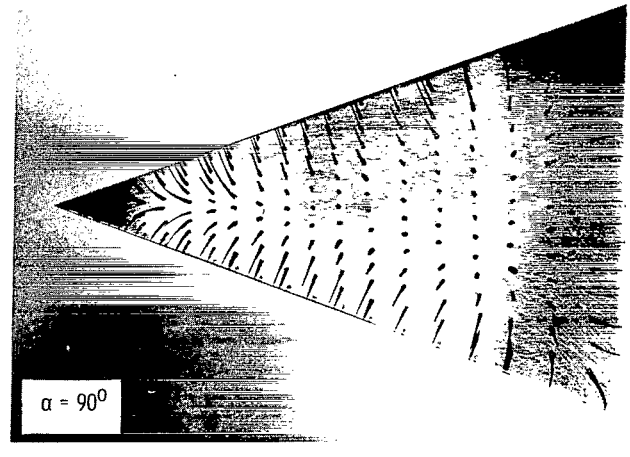

Figure 4.- Surface flow patterns over basic wing. $\delta_n = \delta_f = 0^\circ$. L-64-378

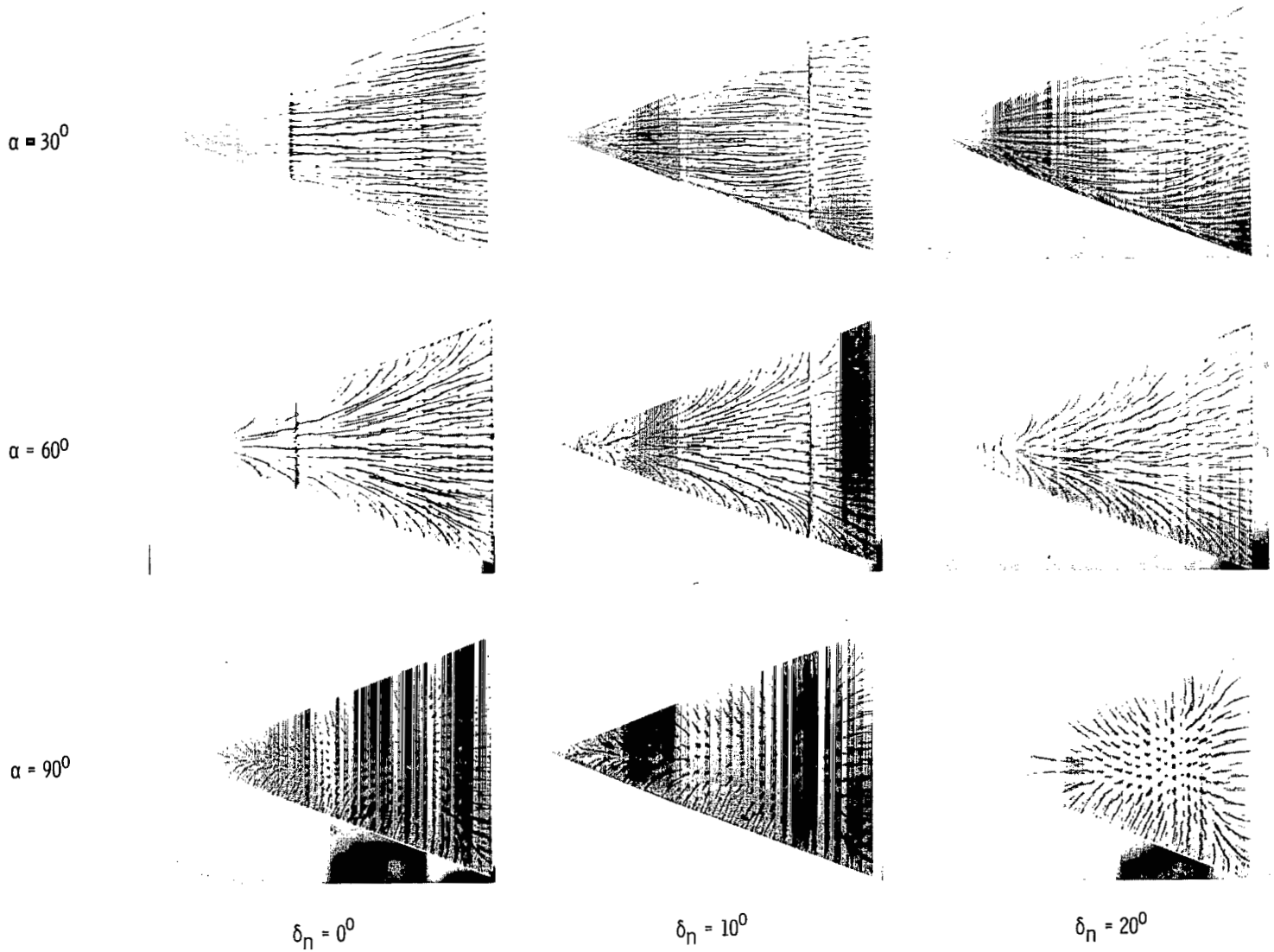

(a) $\delta_f = 0^\circ$.

Figure 5.- Effects of nose incidence on surface flow patterns.

L-64-379

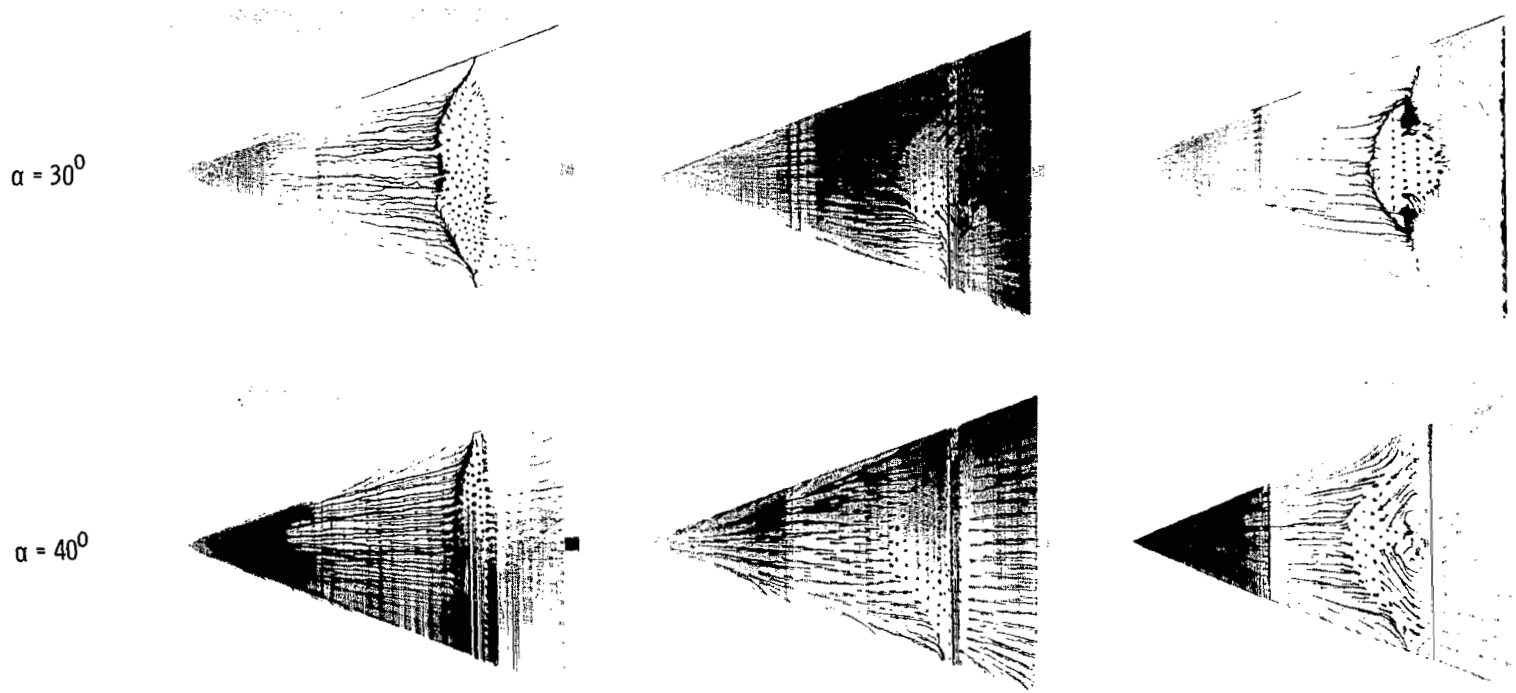

(b) $\delta_f = 10^\circ$.

Figure 5.- Continued.

L-64-380

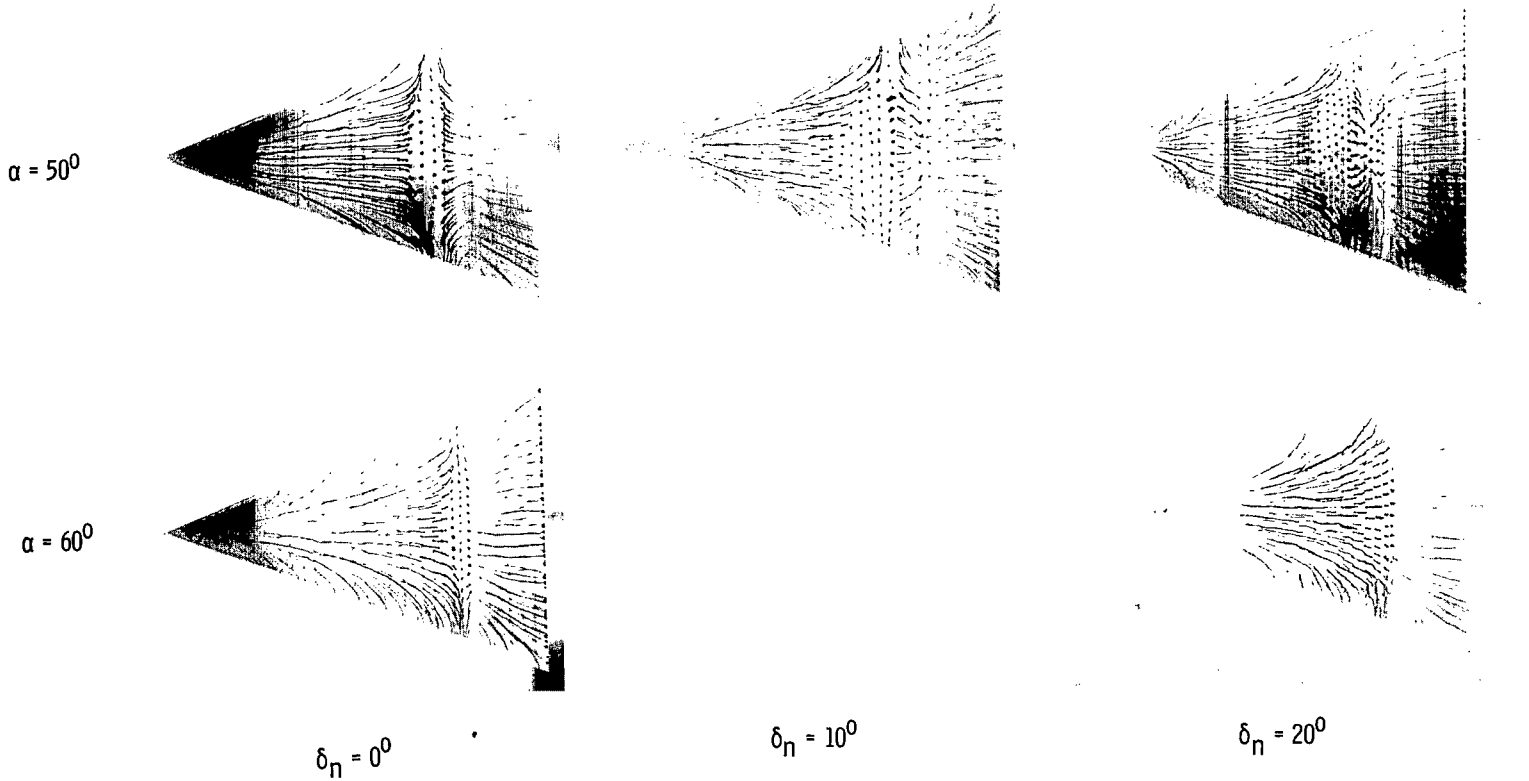

(b) $\delta_f = 10^\circ$. Concluded.

L-64-381

Figure 5.- Continued.

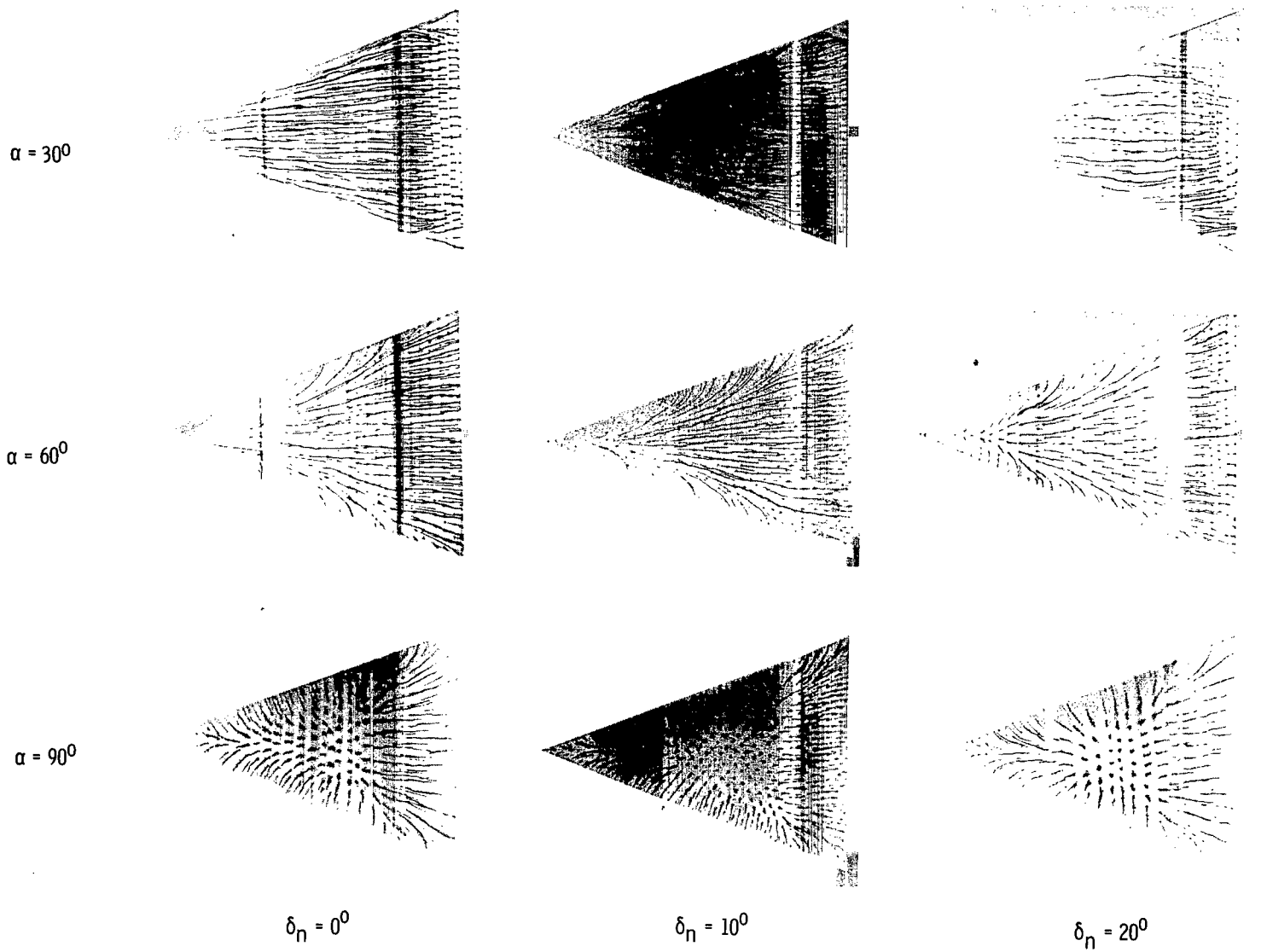

(c) $\delta_f = -30°$.

Figure 5.- Concluded.

L-64-382

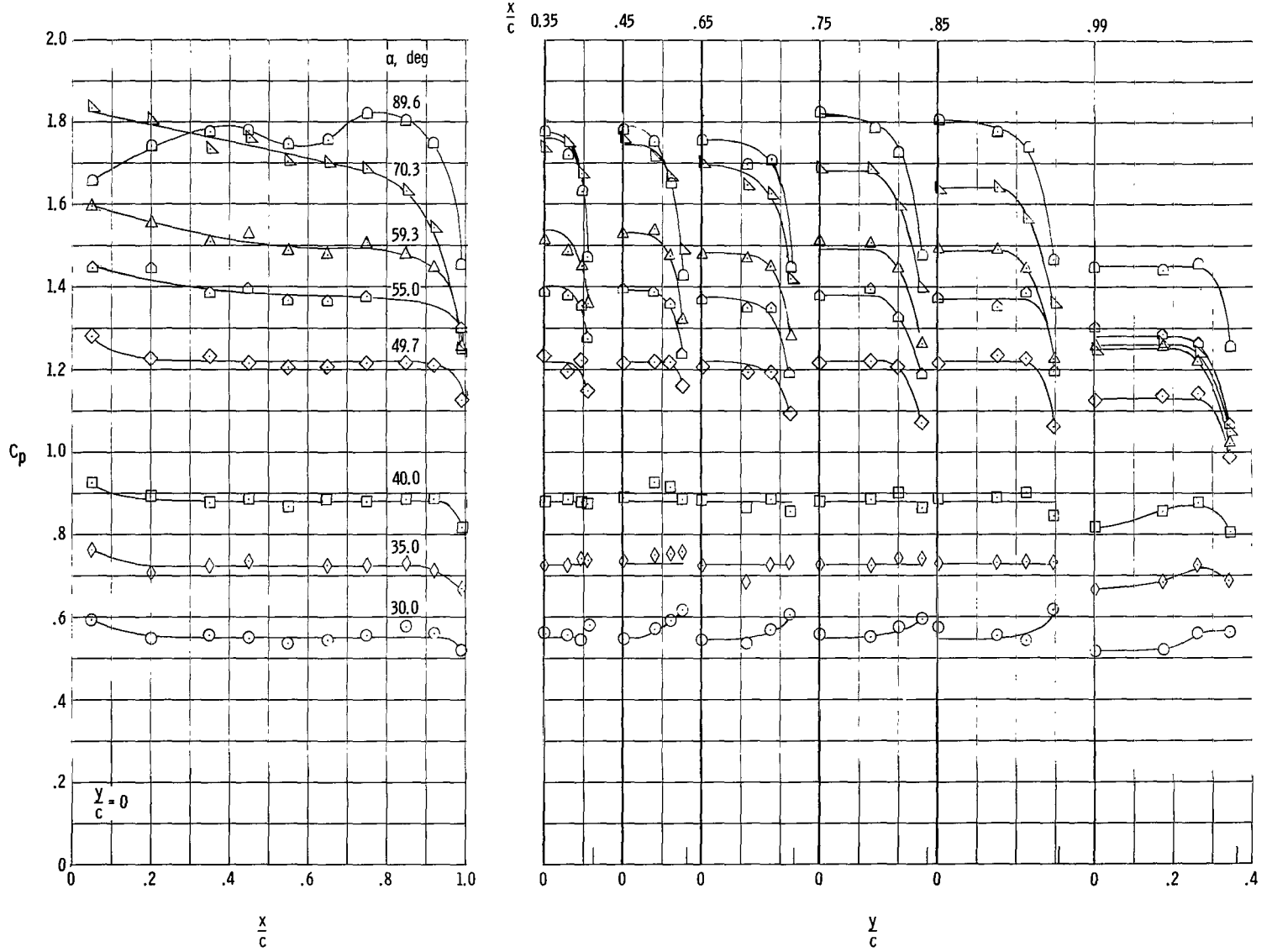

Figure 6.- Pressure distribution over wing. $\delta_n = \delta_f = 0^o$. Tick marks on y/c scale denote leading edge.

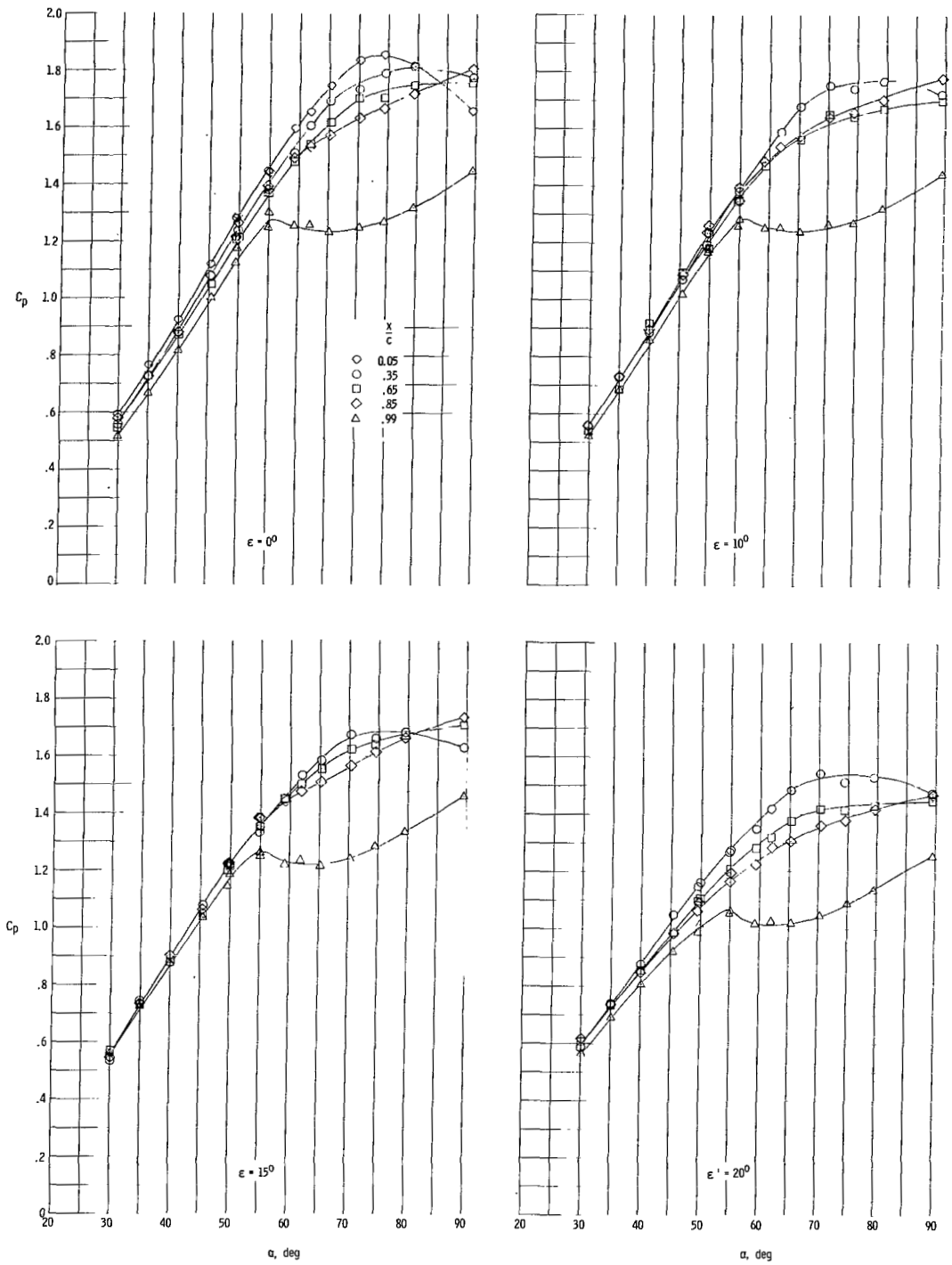

Figure 7.- Variation of pressure coefficient with angle of attack at various locations. $\delta_n = \delta_f = 0^0$.

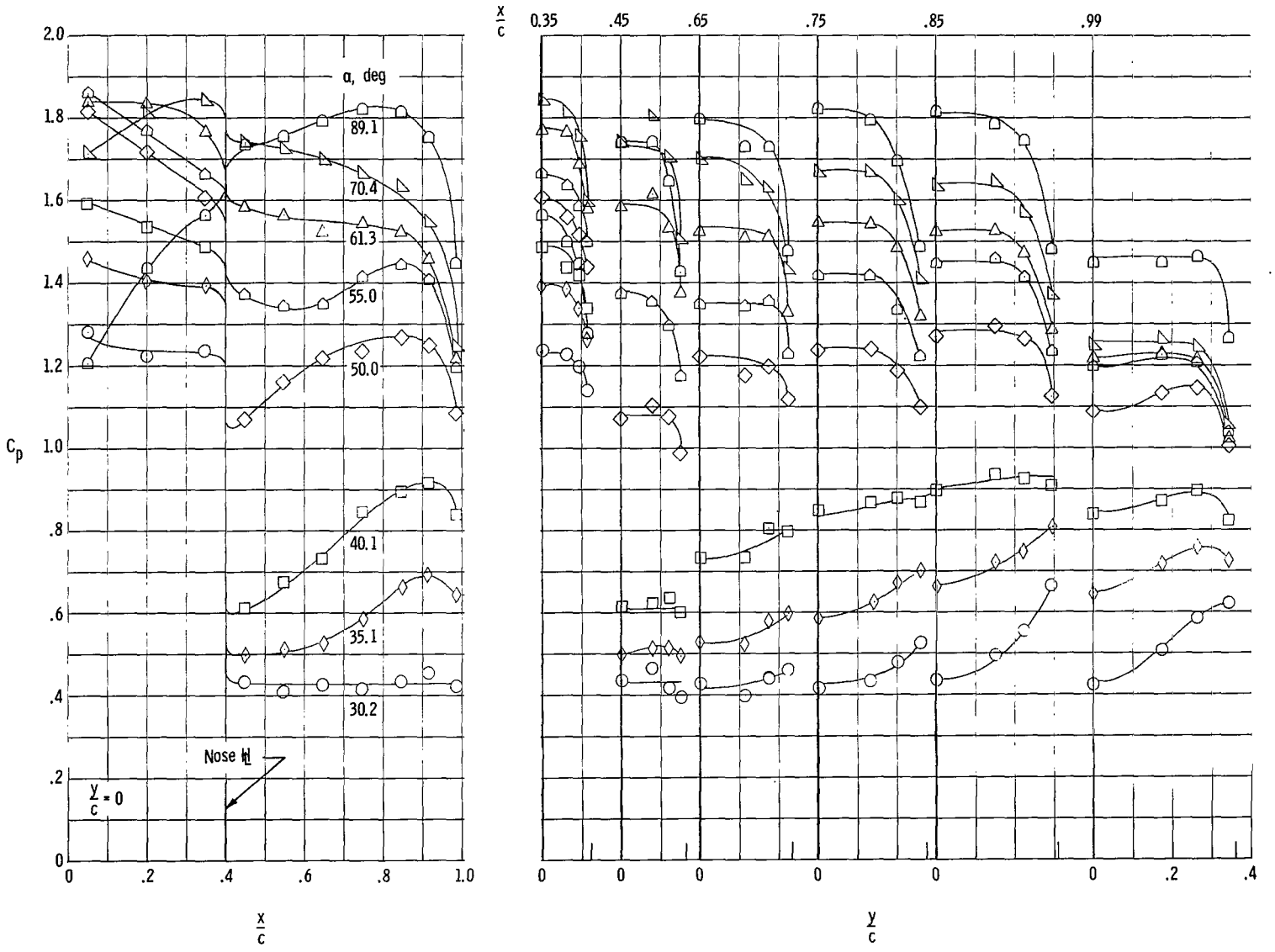

Figure 8.- Pressure distribution over wing. $\delta_n = 20^o$; $\delta_f = 0^o$. Tick marks on y/c scale denote leading edge.

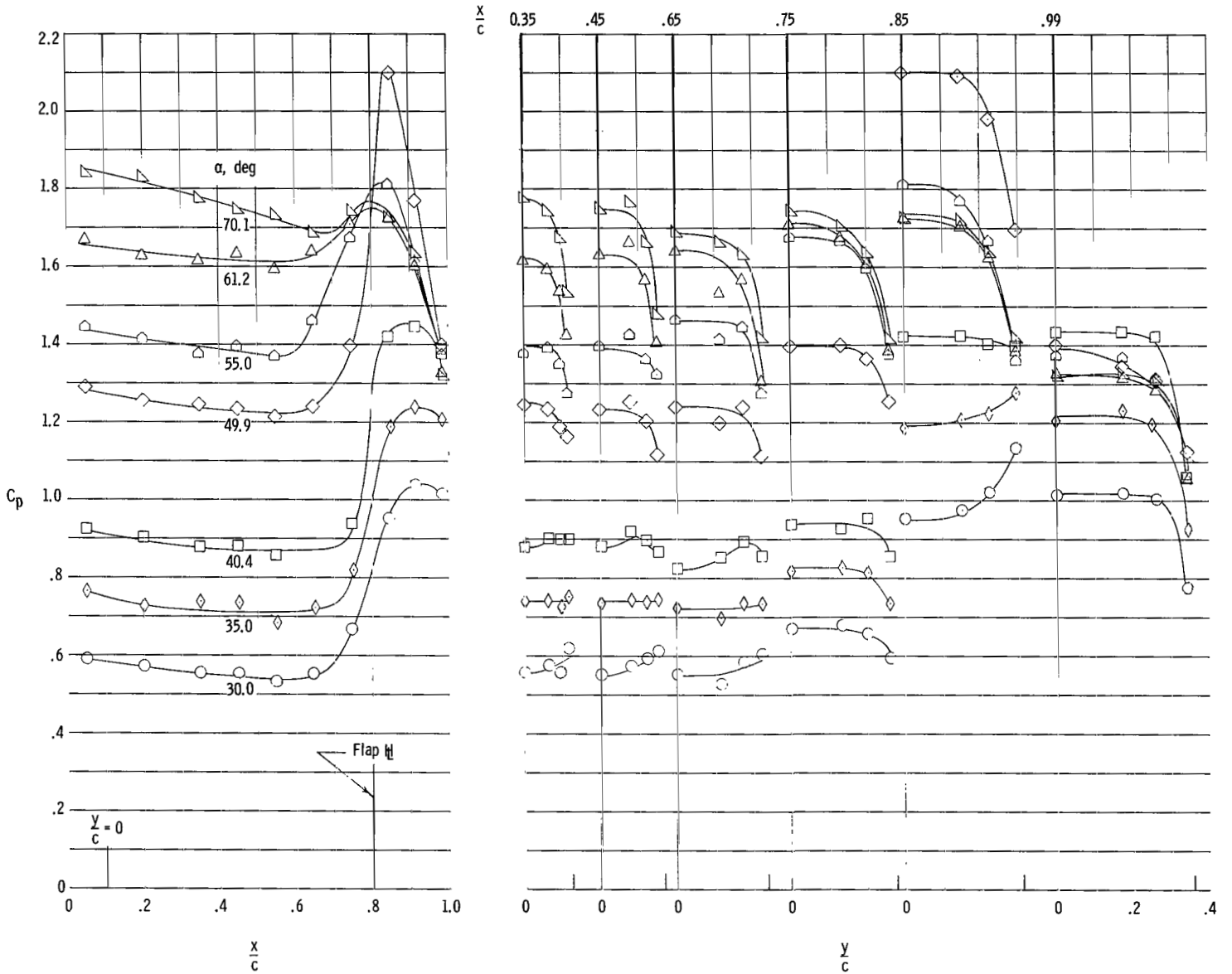

Figure 9.- Pressure distribution over wing. $\delta_n = 0^o$; $\delta_f = 10^o$. Tick marks on y/c scale denote leading edge.

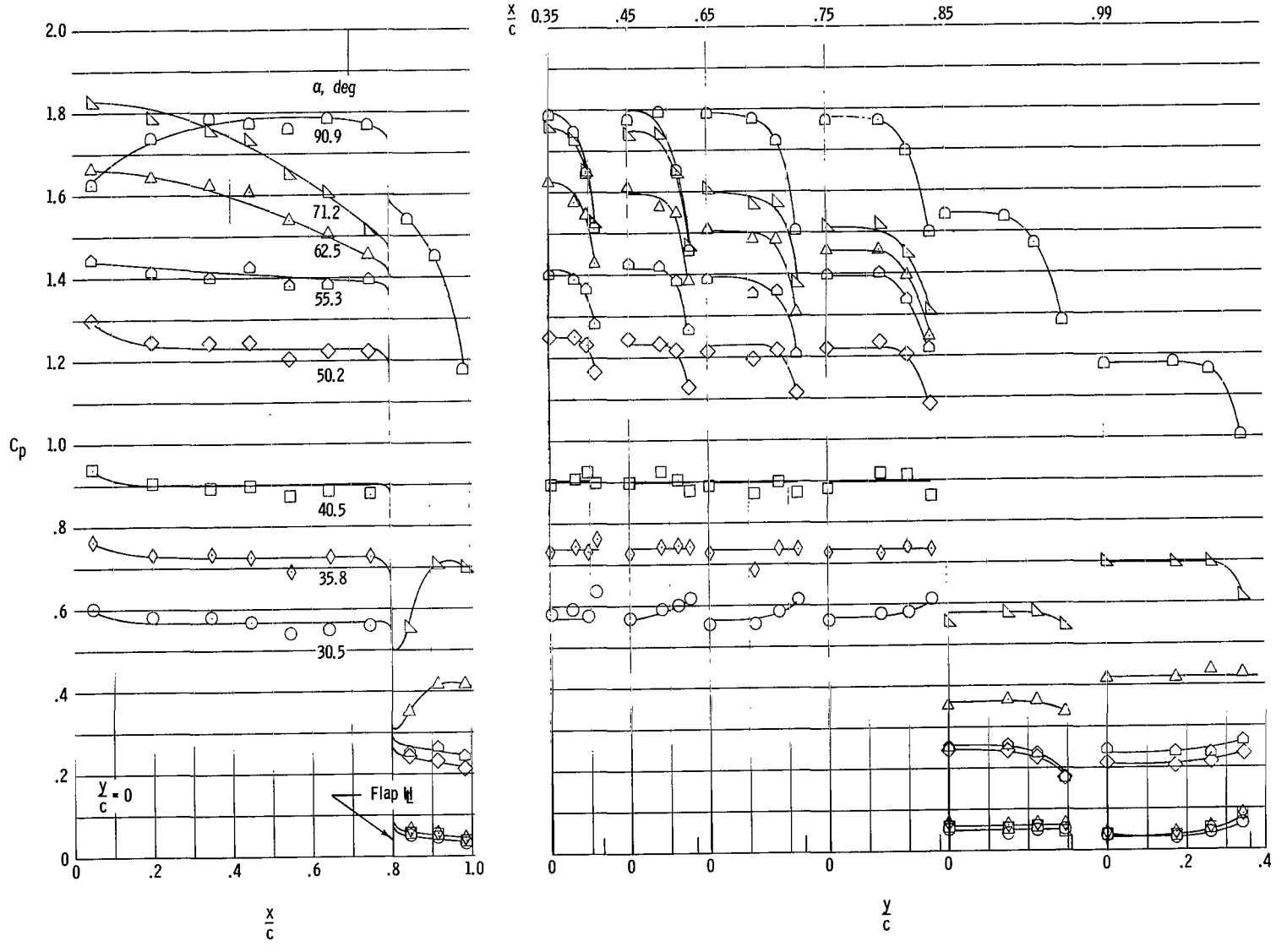

Figure 10.- Pressure distribution over wing. $\delta_n = 0^o$; $\delta_f = -30^o$. Tick marks on y/c scale denote leading edge.

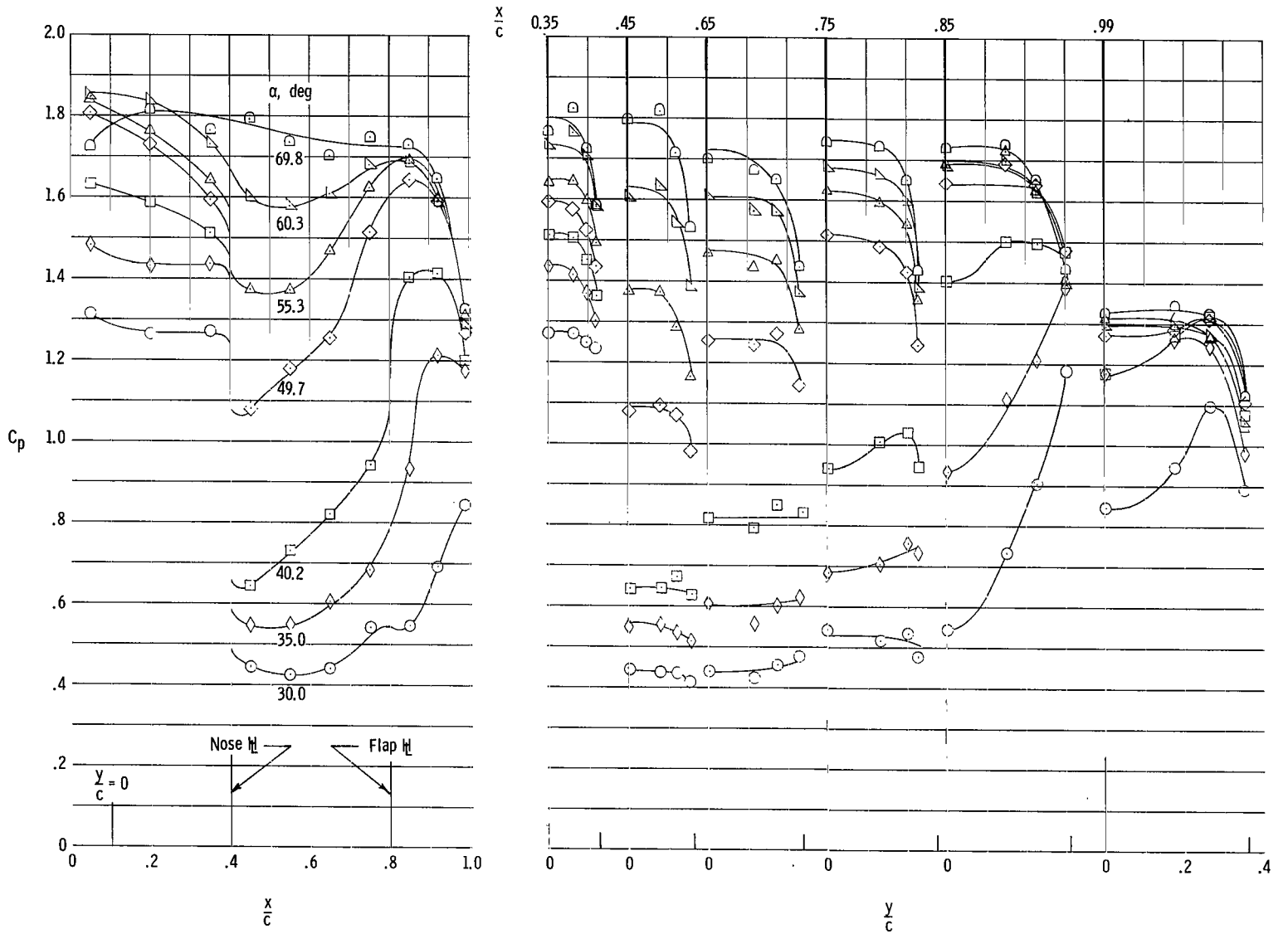

Figure 11.- Pressure distribution over wing. $\delta_n = 20^o$; $\delta_f = 10^o$. Tick marks on y/c scale denote leading edge.

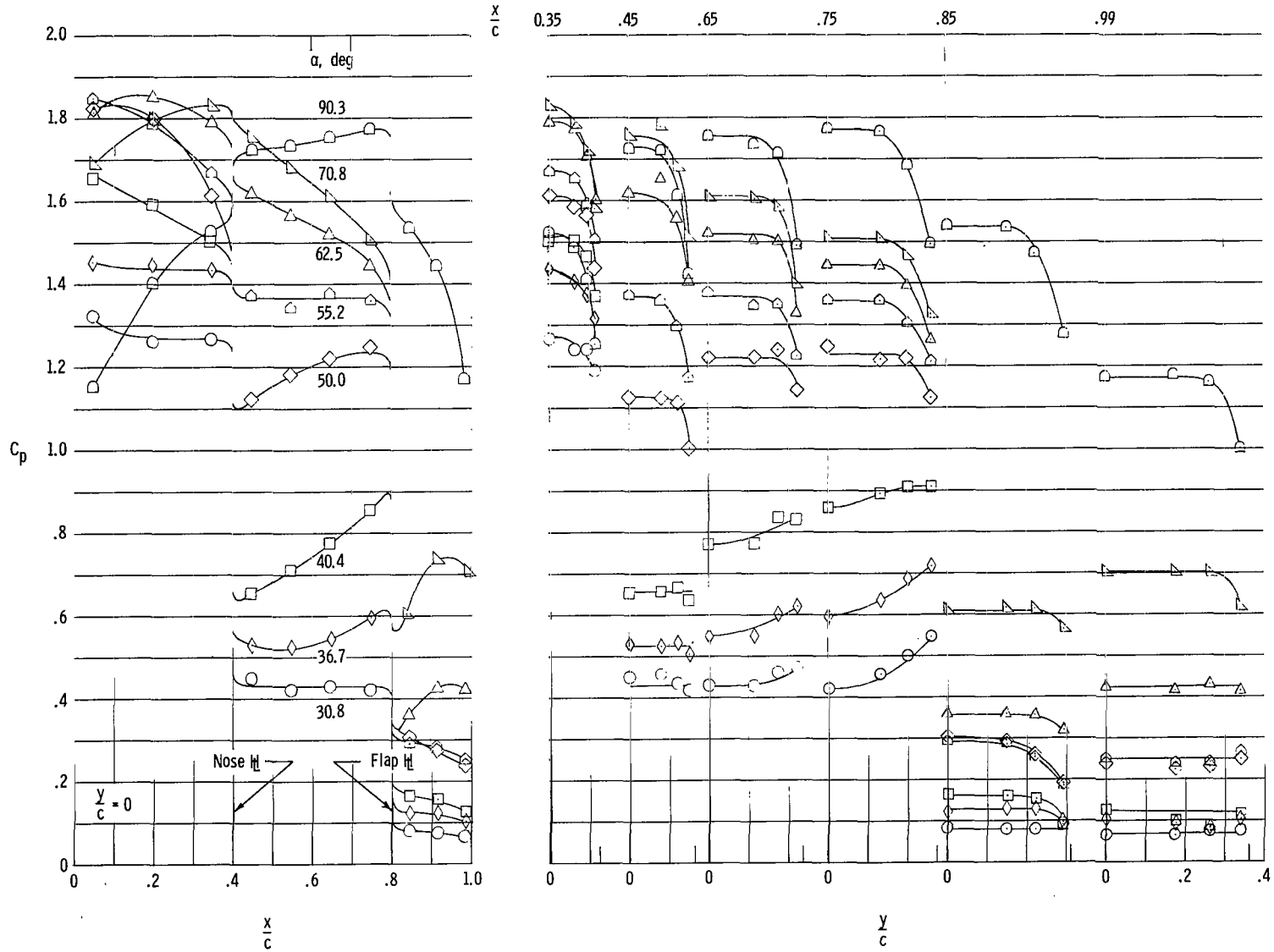

Figure 12.- Pressure distribution over wing. $\delta_n = 20^o$; $\delta_f = -30^o$. Tick marks on y/c scale denote leading edge.

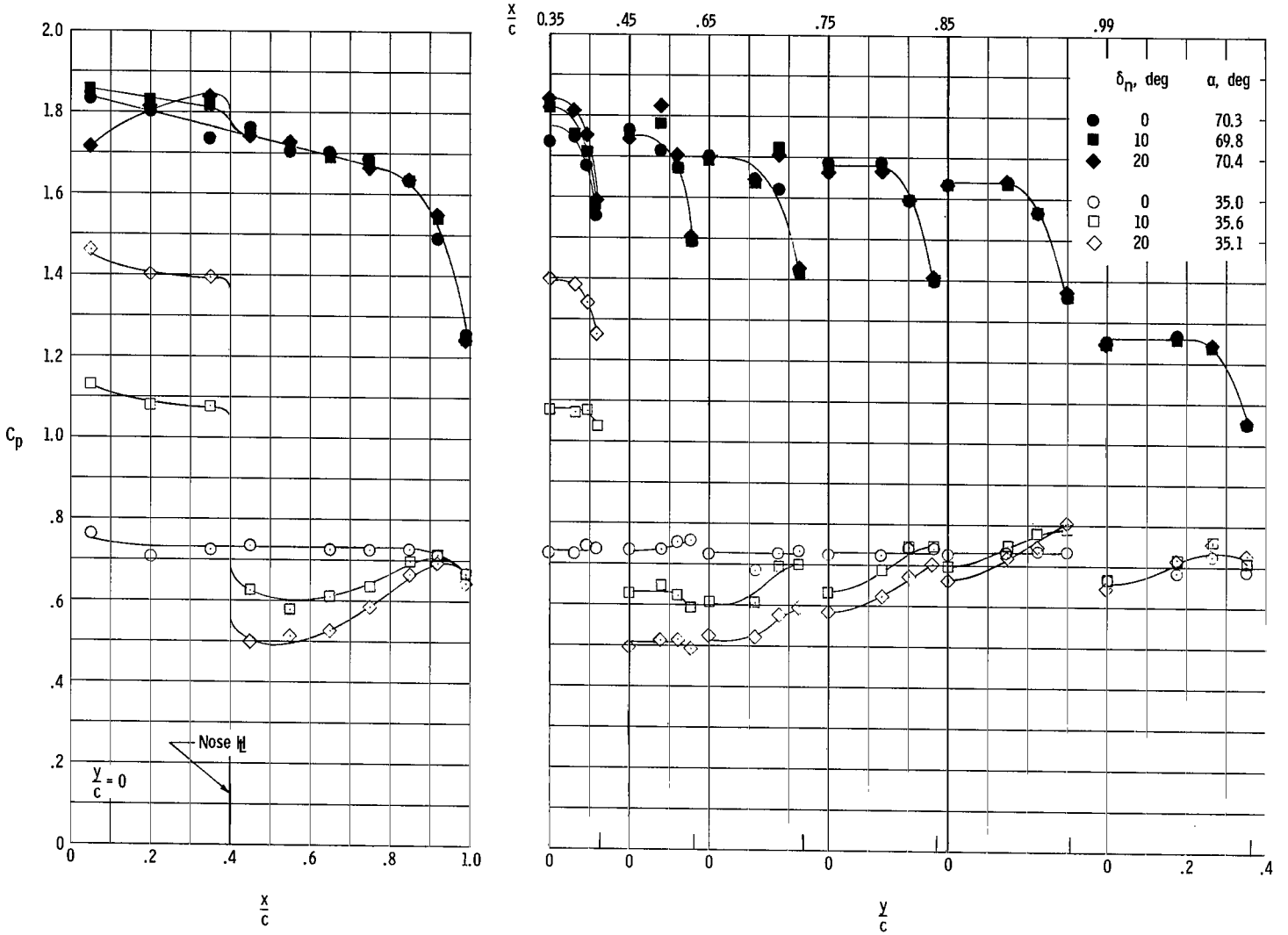

(a) $\delta_f = 0^\circ$.

Figure 13.- Effects of nose incidence on wing pressure distributions at two representative angles of attack. Tick marks on y/c scale denote leading edge.

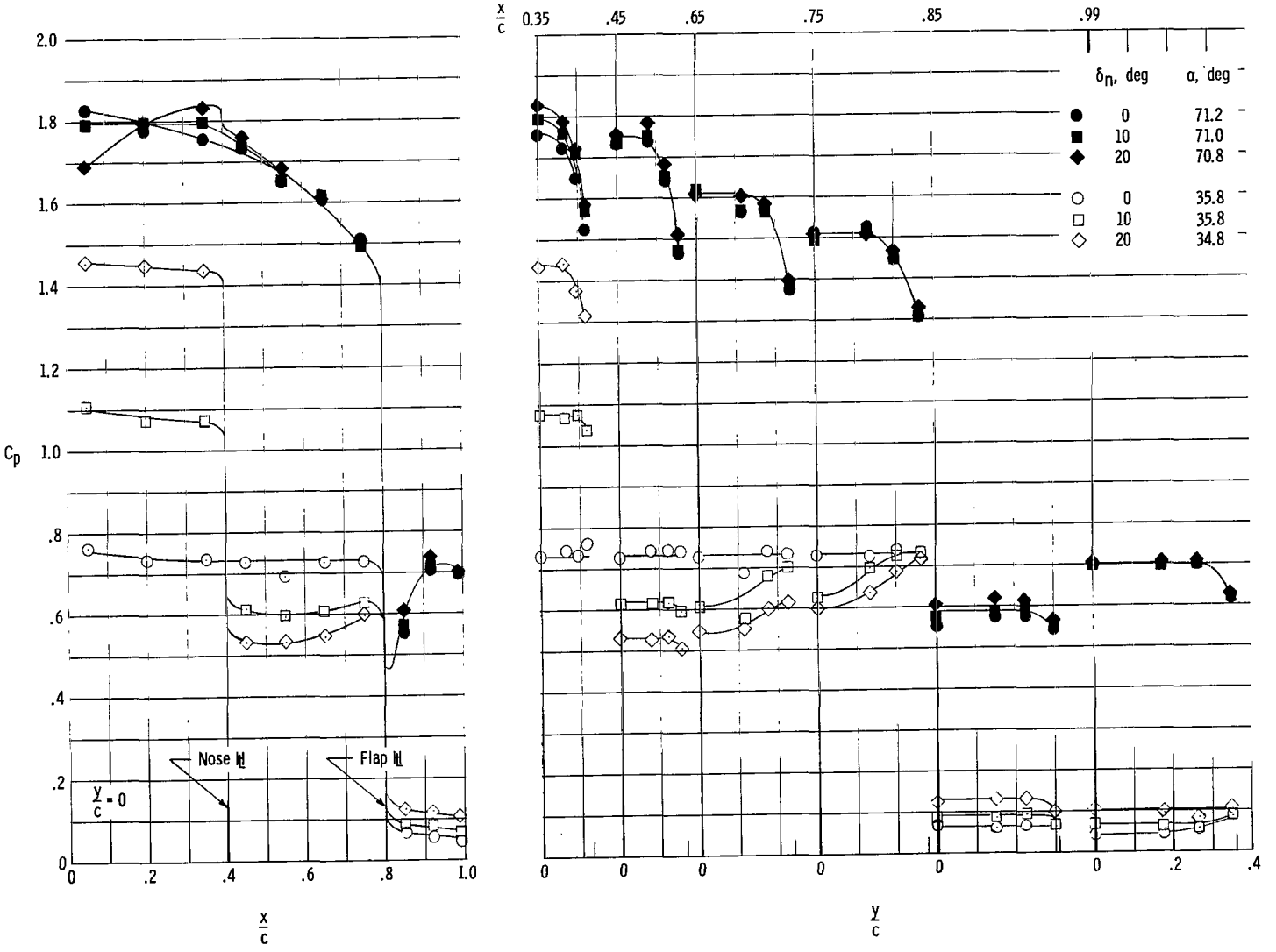

(b). $\delta_f = -30^o$.

Figure 13.- Continued.

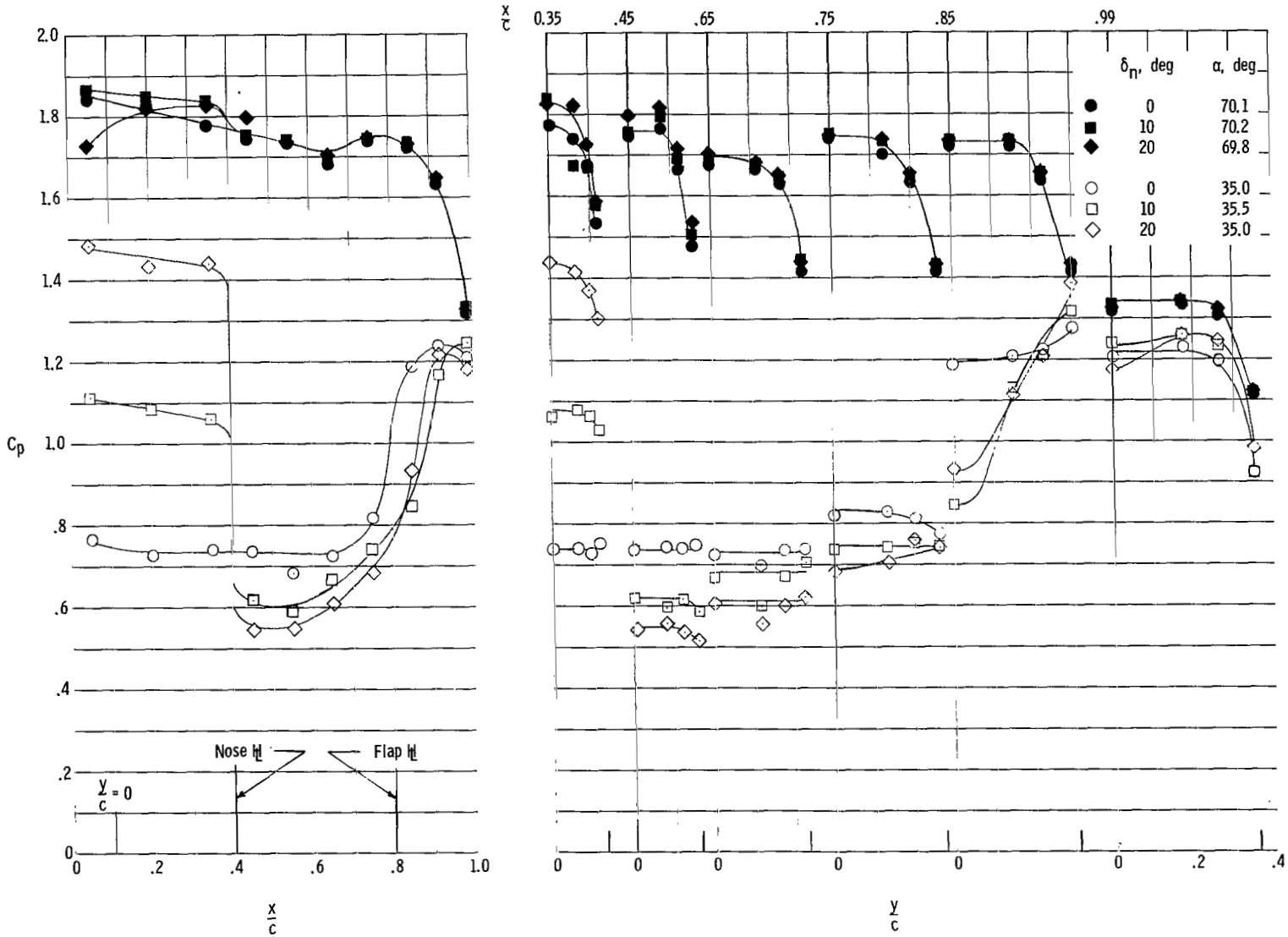

(c) $\delta_f = 10^o$.

Figure 13.- Concluded.

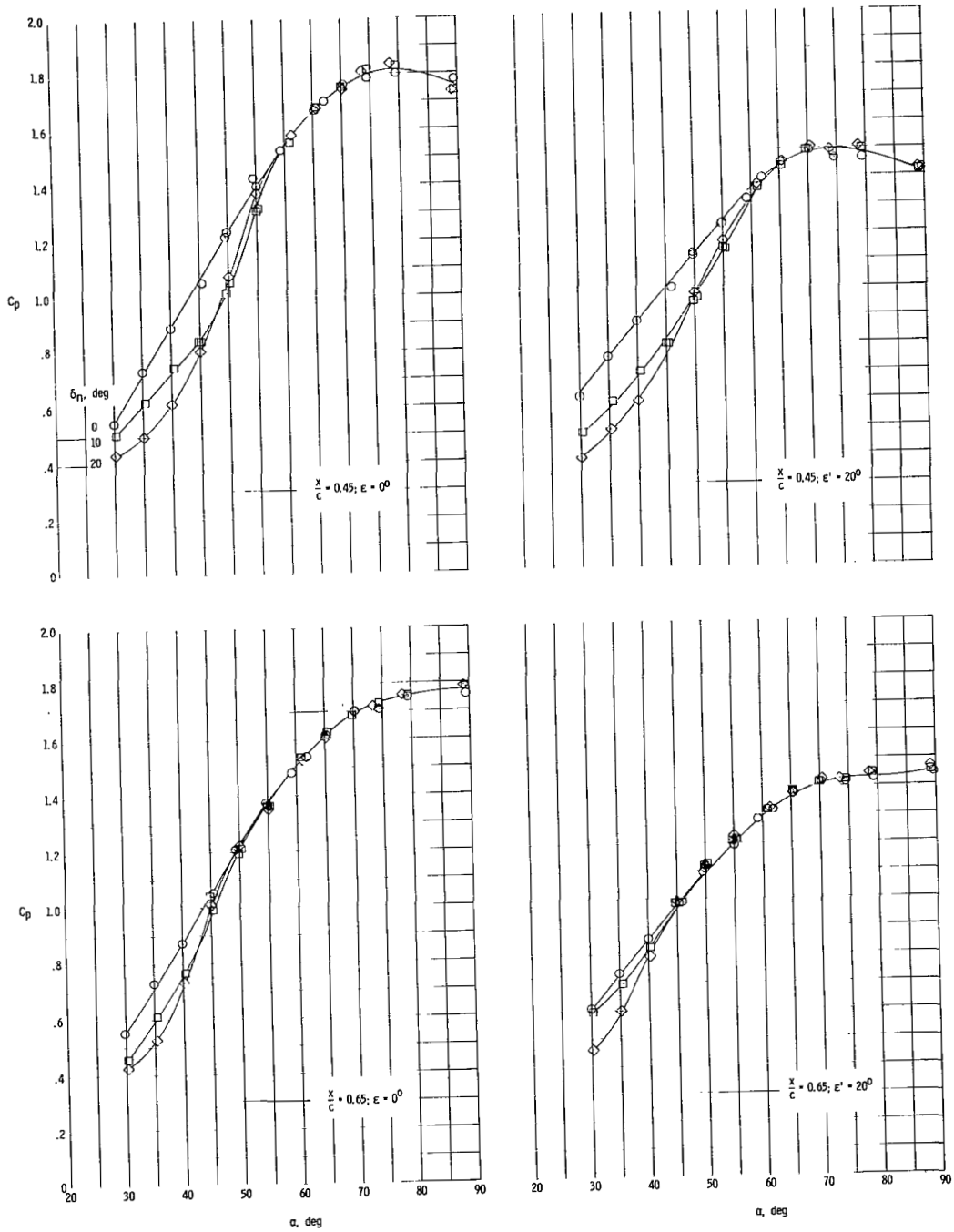

(a) $\delta_f = 0^o$.

Figure 14.- Effect of nose incidence on pressure at various locations as a function of angle of attack.

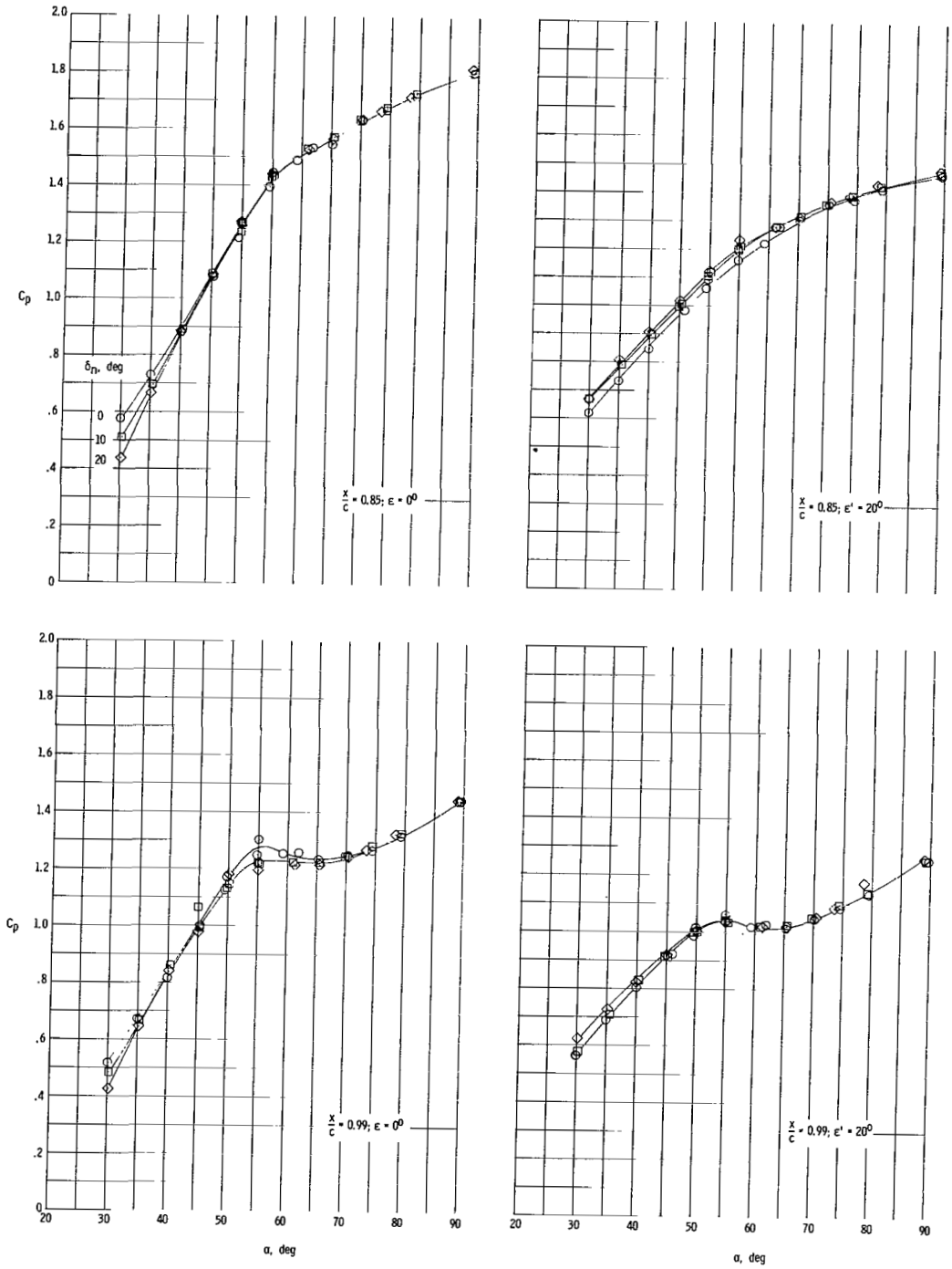

(a) $\delta_f = 0^\circ$. Concluded.

Figure 14.- Continued.

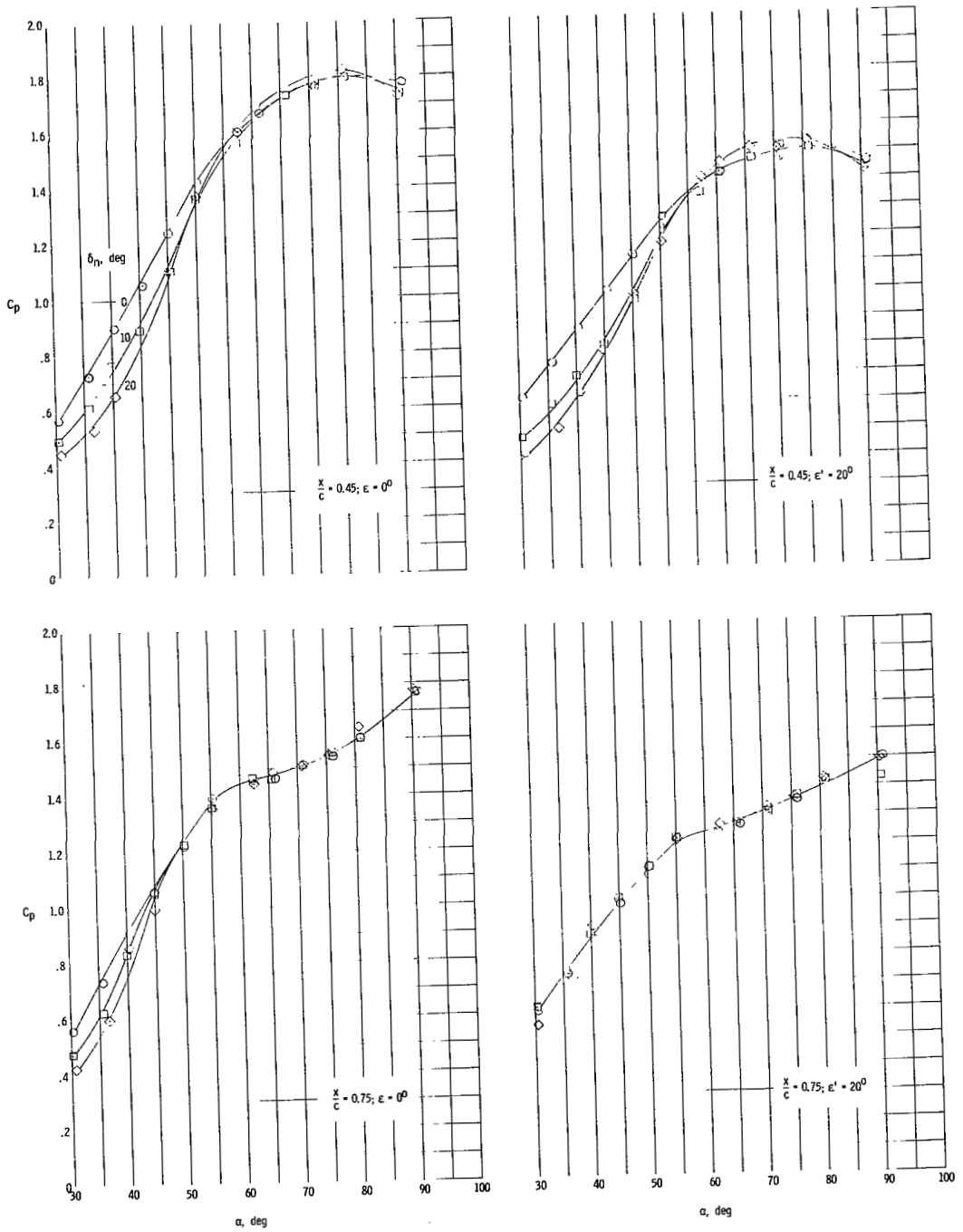

(b) $\delta_f = -30°$.

Figure 14.- Continued.

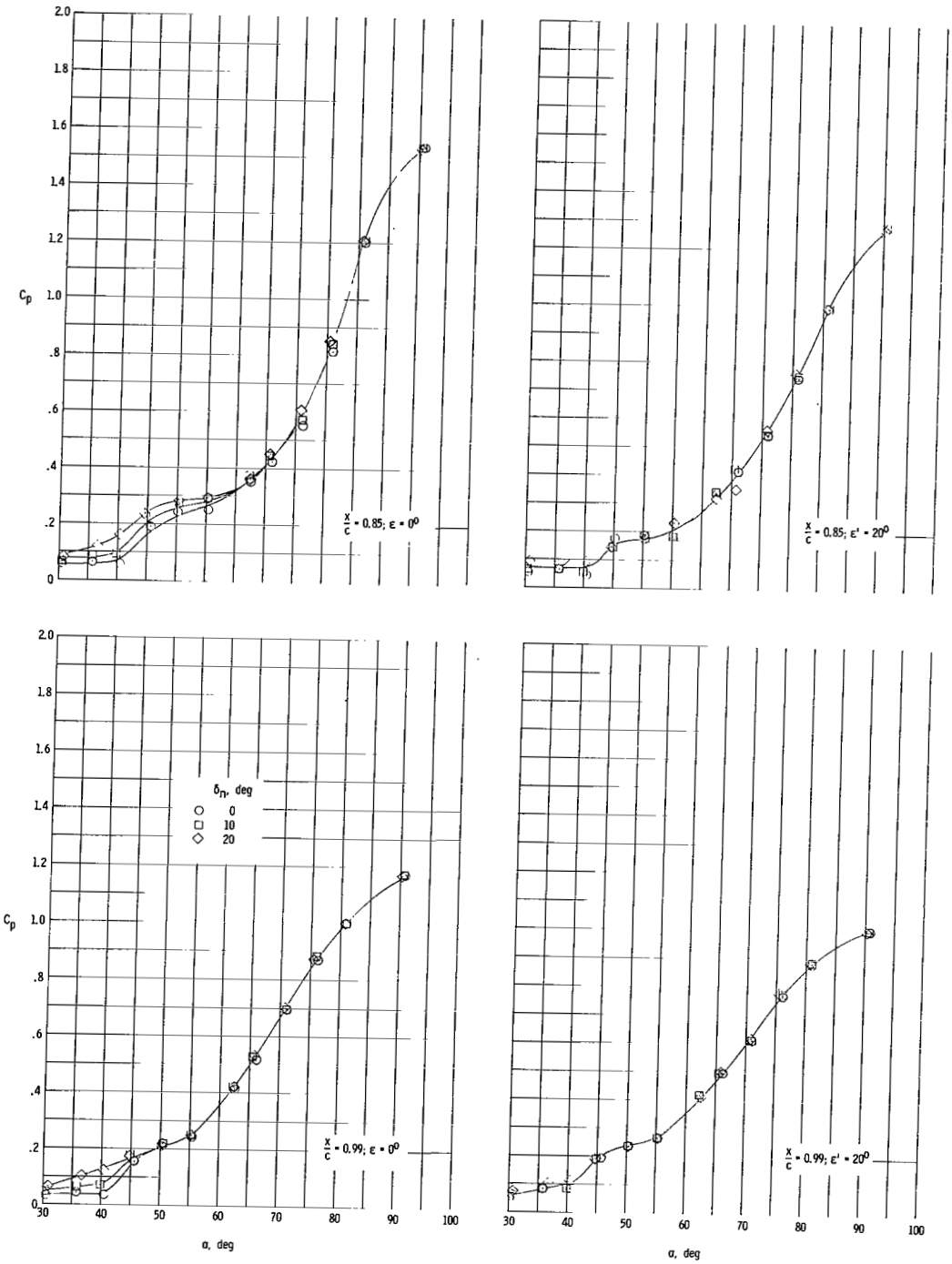

(b) $\delta_f = -30^\circ$. Concluded.

Figure 14.- Continued.

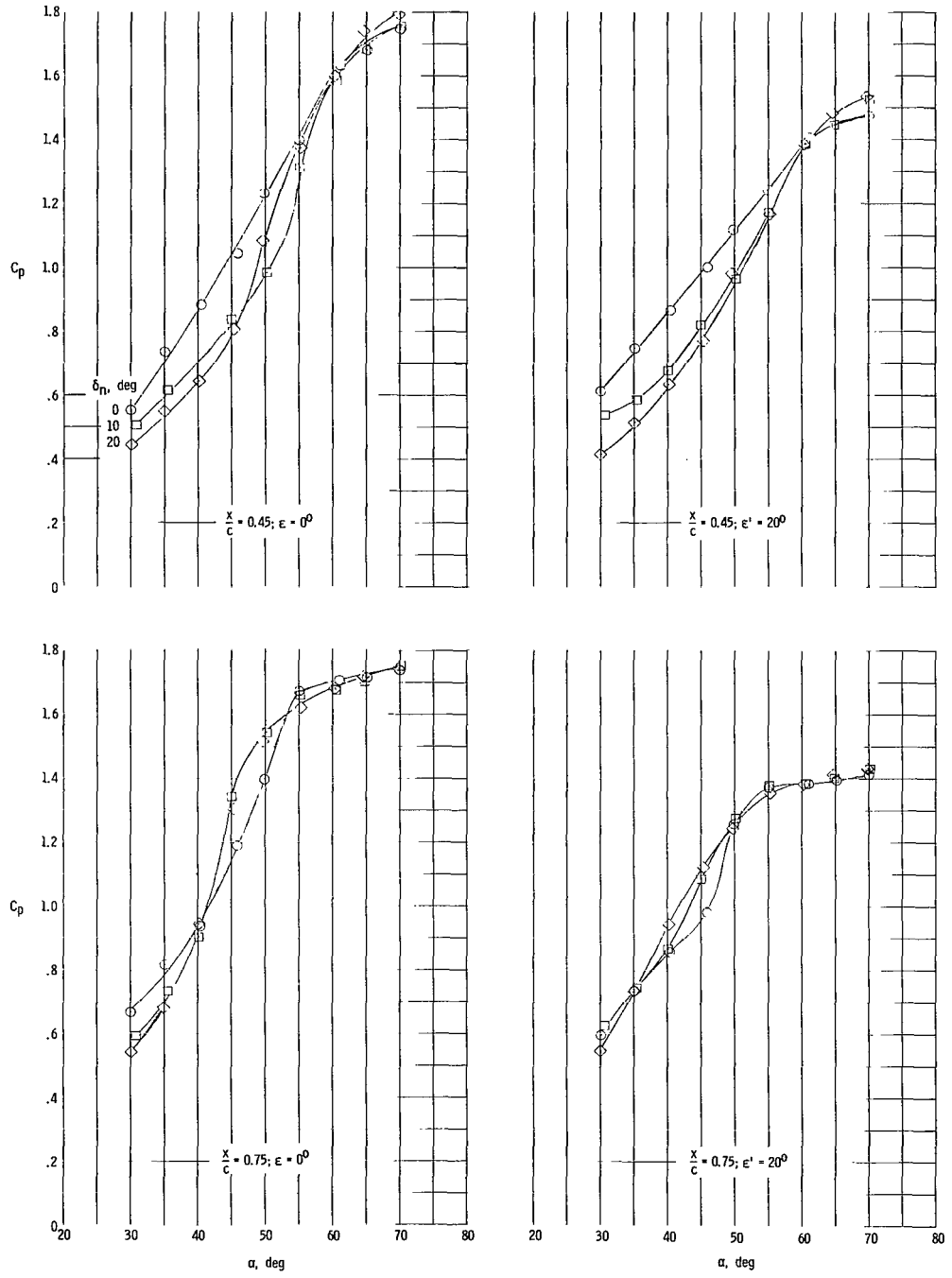

(c) $\delta_f = 10^o$.

Figure 14.- Continued.

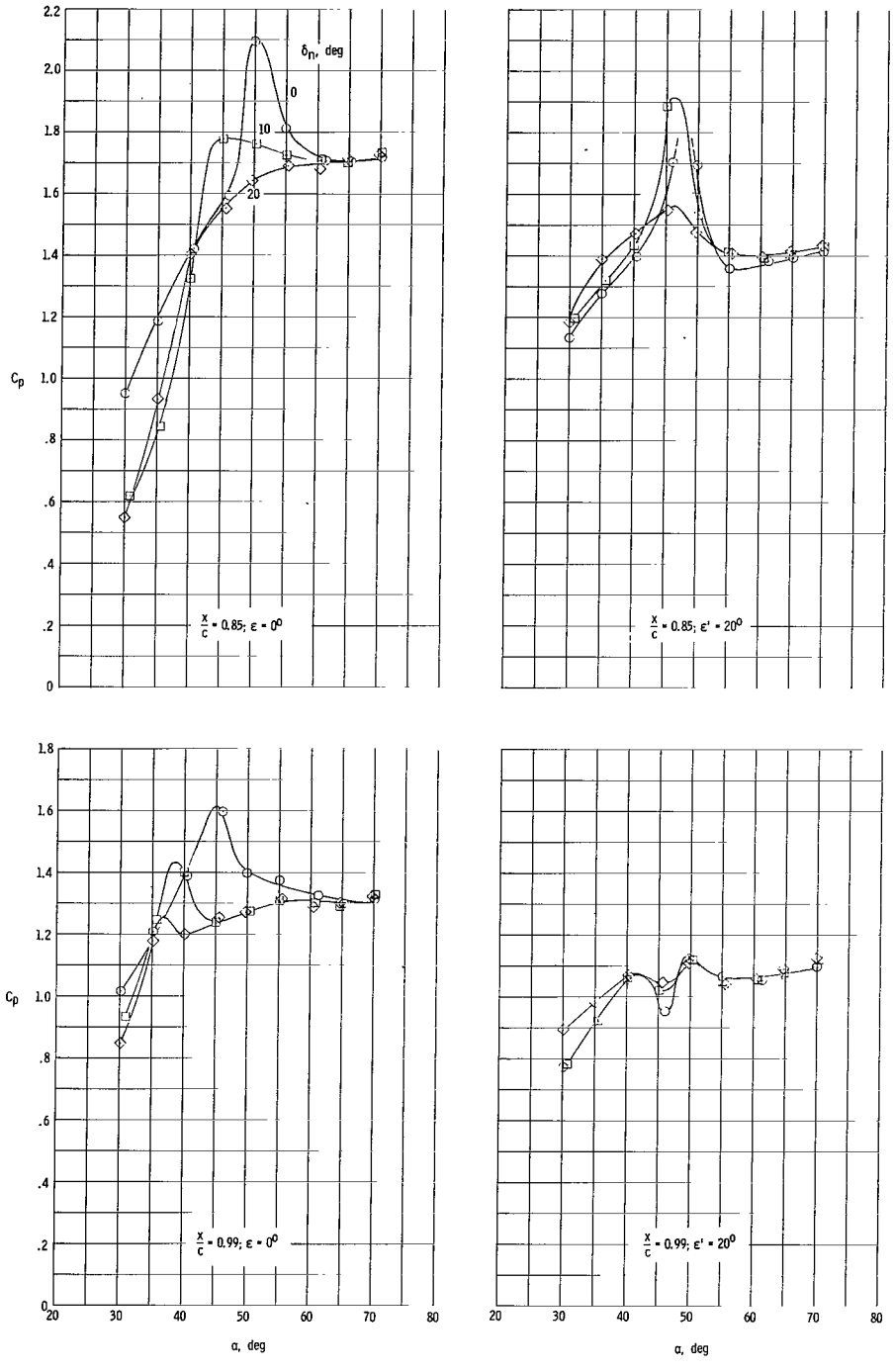

(c) $\delta_f = 10^\circ$. Concluded.

Figure 14.- Concluded.

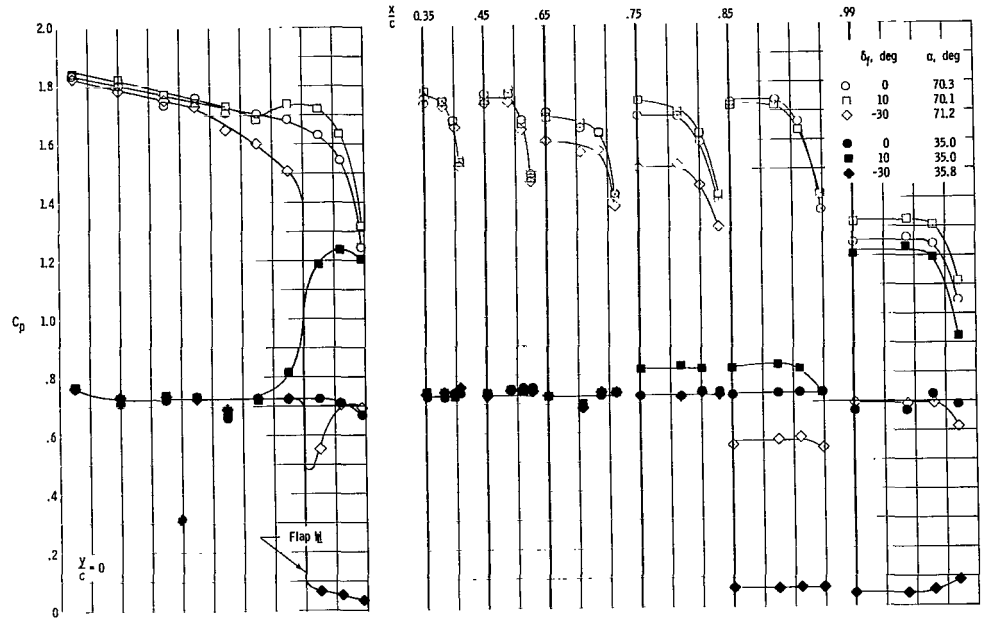

(a) $\delta_n = 0^o$.

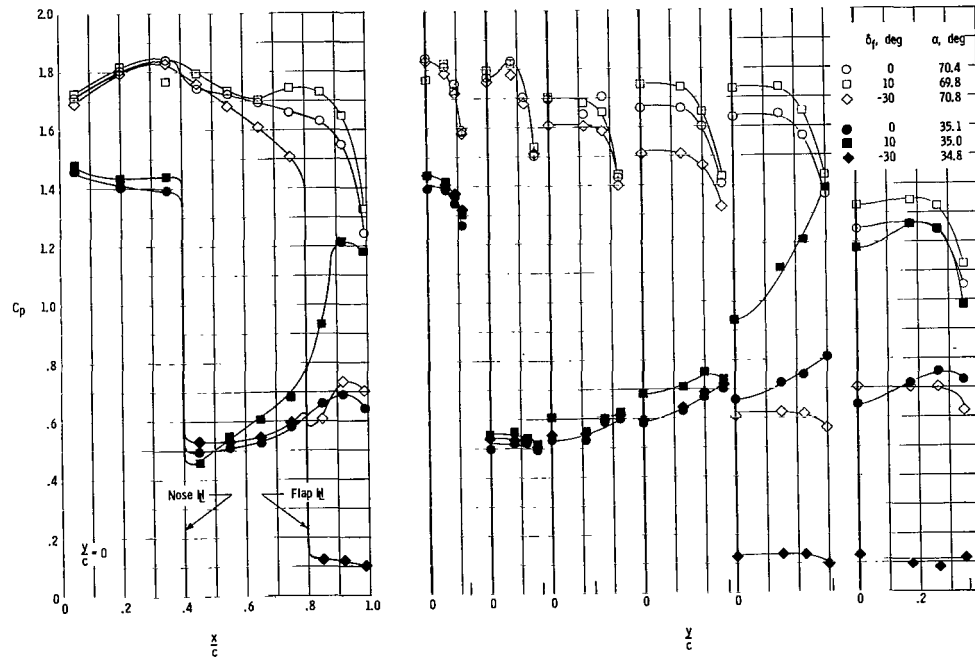

(b) $\delta_n = 20^o$.

Figure 15.- Effect of flap deflection on pressure distribution at two representative angles of attack.

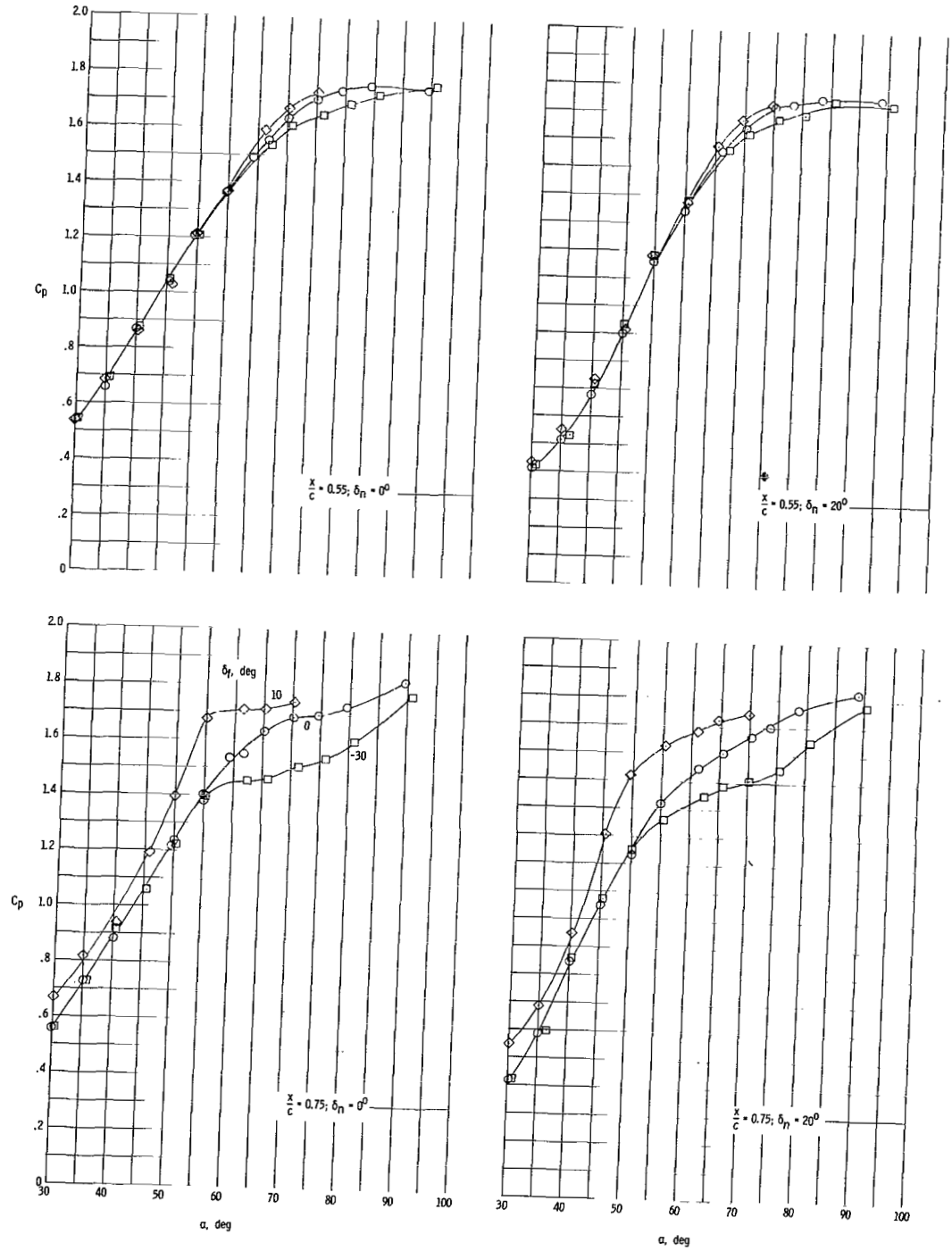

(a) $\epsilon = 0^{\circ}$.

Figure 16.- Effect of flap deflection on pressure at various locations as a function of angle of attack.

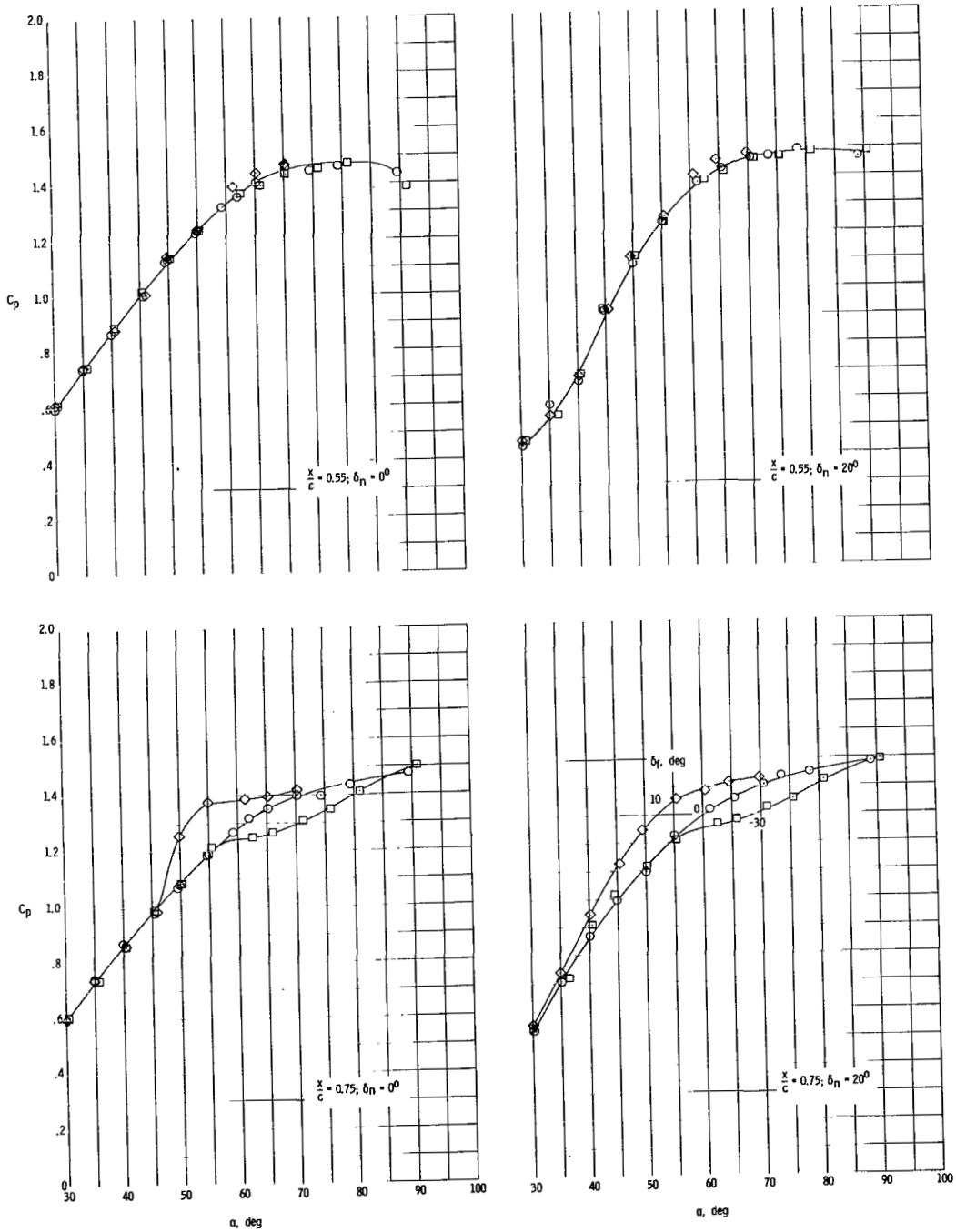

(b) $\epsilon' = 20^o$.

Figure 16.- Concluded.

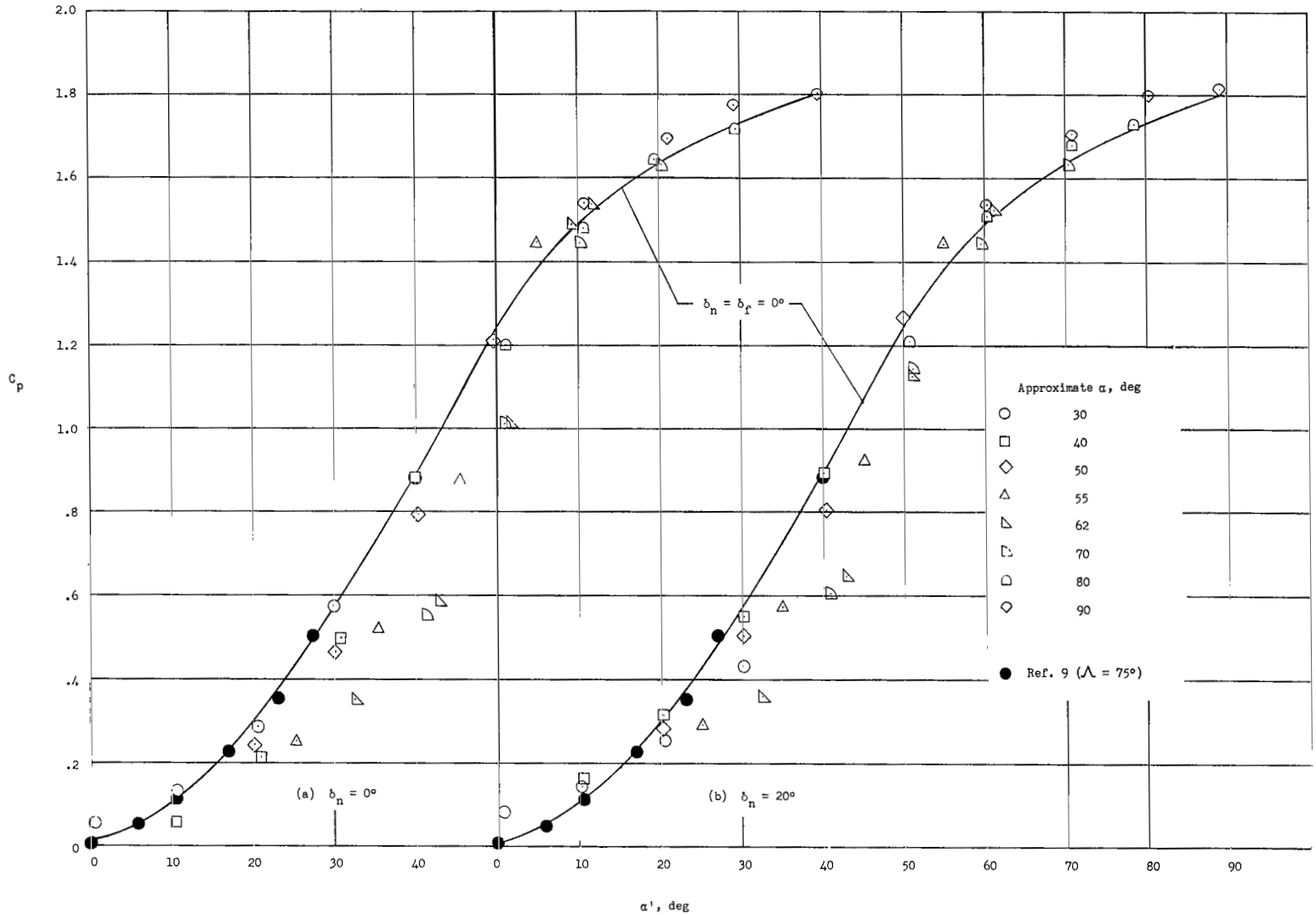

Figure 17.- Carryover effects on flap. x/c = 0.85; y/c = 0.

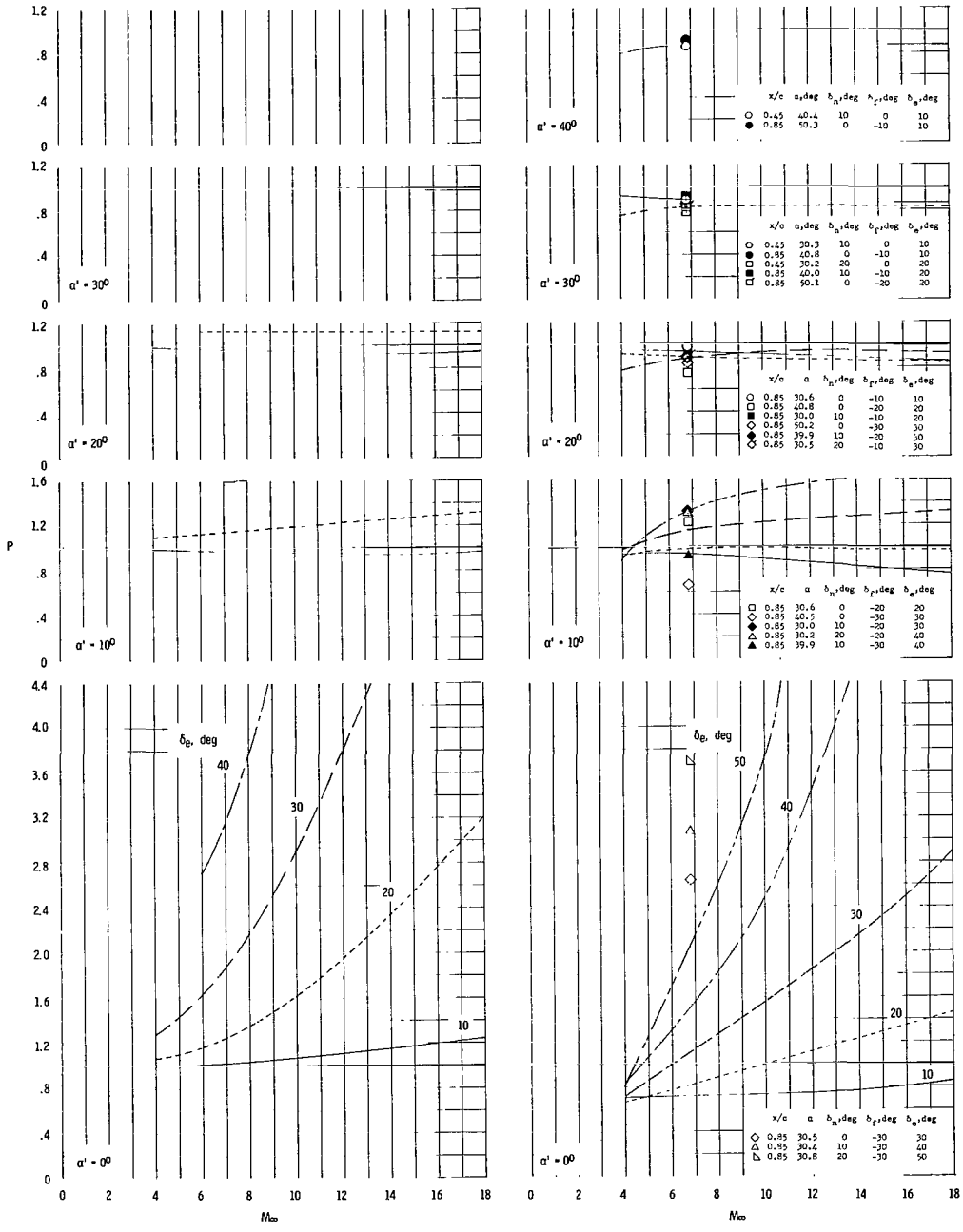

(a) Two-dimensional compression plus two-dimensional expansion.

(b) Conical compression plus two-dimensional expansion.

Figure 18.- Effect of Mach number, expansion angle, and local angle of attack on surface pressure behind an expansion.

"The aeronautical and space activities of the United States shall be conducted so as to contribute . . . to the expansion of human knowledge of phenomena in the atmosphere and space. The Administration shall provide for the widest practicable and appropriate dissemination of information concerning its activities and the results thereof."

—NATIONAL AERONAUTICS AND SPACE ACT OF 1958

NASA SCIENTIFIC AND TECHNICAL PUBLICATIONS

TECHNICAL REPORTS: Scientific and technical information considered important, complete, and a lasting contribution to existing knowledge.

TECHNICAL NOTES: Information less broad in scope but nevertheless of importance as a contribution to existing knowledge.

TECHNICAL MEMORANDUMS: Information receiving limited distribution because of preliminary data, security classification, or other reasons.

CONTRACTOR REPORTS: Technical information generated in connection with a NASA contract or grant and released under NASA auspices.

TECHNICAL TRANSLATIONS: Information published in a foreign language considered to merit NASA distribution in English.

TECHNICAL REPRINTS: Information derived from NASA activities and initially published in the form of journal articles.

SPECIAL PUBLICATIONS: Information derived from or of value to NASA activities but not necessarily reporting the results of individual NASA-programmed scientific efforts. Publications include conference proceedings, monographs, data compilations, handbooks, sourcebooks, and special bibliographies.

Details on the availability of these publications may be obtained from:

SCIENTIFIC AND TECHNICAL INFORMATION DIVISION

NATIONAL AERONAUTICS AND SPACE ADMINISTRATION

Washington, D.C. 20546